



저작자표시-비영리-변경금지 2.0 대한민국

이용자는 아래의 조건을 따르는 경우에 한하여 자유롭게

- 이 저작물을 복제, 배포, 전송, 전시, 공연 및 방송할 수 있습니다.

다음과 같은 조건을 따라야 합니다:



저작자표시. 귀하는 원저작자를 표시하여야 합니다.



비영리. 귀하는 이 저작물을 영리 목적으로 이용할 수 없습니다.



변경금지. 귀하는 이 저작물을 개작, 변형 또는 가공할 수 없습니다.

- 귀하는, 이 저작물의 재이용이나 배포의 경우, 이 저작물에 적용된 이용허락조건을 명확하게 나타내어야 합니다.
- 저작권자로부터 별도의 허가를 받으면 이러한 조건들은 적용되지 않습니다.

저작권법에 따른 이용자의 권리는 위의 내용에 의하여 영향을 받지 않습니다.

이것은 [이용허락규약\(Legal Code\)](#)을 이해하기 쉽게 요약한 것입니다.

[Disclaimer](#)

# Chemically Engineered 3D Graphene Nanostructures

The background features a large, light gray watermark of the UNIST logo. It consists of a circular emblem with the text 'UNIST NATIONAL INSTITUTE OF SCIENCE AND TECHNOLOGY' around the perimeter. Inside the circle is a shield-shaped emblem containing a stylized globe and a molecular structure. Below the shield is a trapezoidal base with the letters 'UNIST' on it.

Young-Eun Shin

Chemical Engineering Program

School of Nano-Bioscience and Chemical Engineering

Graduate School of UNIST

2013

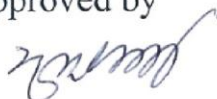
# Chemically Engineered 3D Graphene Nanostructures

A thesis submitted to the School of Nano-Bioscience  
and Chemical Engineering and the Graduate School of UNIST  
in partial fulfillment of the  
requirements for the degree of  
Master of Science

Young-Eun Shin

06. 26. 2013 Month/Day/Year of submission

Approved by



---

Major Advisor

Hyunhyub Ko

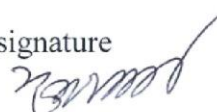
# Chemically Engineered 3D Graphene Nanostructures

Young-Eun Shin

This certifies that the thesis of Young-Eun Shin is approved.

06. 26. 2013 Month/Day/Year of submission

signature



---

Hyunhyub Ko

signature



---

Joon Hak Oh

signature



---

Chang Young Lee

## **Abstract**

Chemically Engineered 3D Graphene Nanostructures, 2013, Young-Eun Shin, Graduate program of Chemical Engineering, Ulsan National Institute of Science and Technology (UNIST)

Recently, 3D graphene nanostructures have attracted considerable attentions for a variety of applications in sensors, separations, lithium-ion batteries, and supercapacitors because of their prominent properties such as high surface area, high electrical conductivity, and thermal/mechanical stability. Herein, we demonstrate various types of 3D graphene nanostructures via chemical modification of graphene oxide and their self-assembly behaviors in different solvent conditions. In particular, porous graphene nanostructures are fabricated through the control of electrostatic repulsions between chemically modified graphene sheets. Chemically reduced graphene oxide sheets are well-dispersed owing to the electrostatic repulsion at high pH condition, while agglomerating each other at low pH condition. Noticeably, we fabricate different graphene morphologies such as dendrite-like structure and wire-like structure by controlling the pH condition. In addition, different morphology of graphene nanostructures such as crumpled and scrolled geometries is demonstrated via control of pH condition and graphene reduction time. These various type of graphene nanostructures could be used for variety of applications as mentioned above.



## List of Figures

**Figure 1** Carbon-based materials modified with a graphene sheet as a 2D basic building block; Fullerene (0D), Carbon Nanotube (1D), Graphite (3D)<sup>1</sup> (Geim and Novoselov, *Nat. Mater.* **2007**, 6, 183)

**Figure 2** Chemical approach of aqueous graphene dispersion. (1) Oxidation of graphite to graphite oxide with increased interlayer distance. (2) Exfoliation of graphite oxide in aqueous solution by sonication to obtain GO colloids which are stabilized by electrostatic repulsion. (3) Controlled conversion of GO colloids to conducting graphene colloids through chemical reduction using hydrazine.<sup>2</sup> (Li et al., *Nat. Nanotechnol.* **2008**, 3, 101)

**Figure 3** Structure of graphene derivatives synthesized by oxidation and reduction.<sup>3</sup> (Cote et al., *Pure Appl. Chem.* **2011**, 83, 95)

**Figure 4** Different morphology of carbon-based materials such as graphene, CNT, graphene nano scroll (GNS), graphene nano ribbon.<sup>4,5</sup> (Kosynkin et al., *Nature* **2009**, 458, 872; Braga et al., *Nano Lett.* **2004**, 4, 881)

**Figure 5** Fabrications for graphene thin films; (a) drop casting, (b) spin coating, (c) Langmuir-Blodgett assembly<sup>6</sup>, (d) dip casting, (e) rod coating, (f) spray coating, (g) inkjet printing<sup>7</sup>. (Kim et al., *Materials today*, **2010**, 13, 28; Bonaccorso et al., *Materials today*, **2012**, 15, 564)

**Figure 6** Various approaches for porous graphene structures. (a) Schematic illustration of the synthesis procedures of the porous graphene foams using silica templates<sup>8</sup> (Huang et al., *Adv. Mater.* **2012**, 24, 4419), (b) SEM image of hierarchically porous graphene structure using bubble templates<sup>9</sup> (Xiao et al., *Nano Lett.* **2011**, 11, 5071), (c) Schematic procedures of preparing graphene sheets-CNTs electrode<sup>10</sup> (Yang et al., *J. Mater. Chem.* **2011**, 21, 2374), (d) SEM image of the ultrathin graphite foam with micropores; inset: photograph of this foam<sup>11</sup> (Ji et al., *Nano Lett.* **2012**, 12, 2446), (e-h)

Morphology of rGO encapsulated sulfur synthesized via oil-water system, (e-f) SEM, (g) TEM, and (h) HRTEM images of this porous structure<sup>12</sup> (Zhang et al., *J. Mater. Chem.* **2012**, 22, 11452).

**Figure 7** Graphene nanoscroll (GNS) with various approaches; (a) Chemical route for GNS with exfoliation/sonication process and (b-d) TEM images of GNS<sup>13</sup> (Viculis et al., *Science* **2003**, 299, 1361); (e) Microwave spark assistance in liquid nitrogen for GNS, (f-g) TEM and SEM images with GNS<sup>14</sup> (Zheng et al., *Adv. Mater.* **2011**, 23, 2460); (h) Mechanical exfoliation using isopropyl alcohol (IPA) for GNS, (i-j) Optical microscope images of (i) graphene sheet and (j) scrolled graphene sheet<sup>15</sup> (Xie et al., *Nano Lett.* **2009**, 9, 2565).

**Figure 8** Analysis of chemically modified graphene. (a) AFM image of GO; the height and the width of GO sheet is below 1nm and 1 $\mu$ m, (b) UV-vis spectra of GO and rGO; red-shift appears after reduction, (c) Raman spectra of GO and rGO with increased  $I_D/I_G$  ratio.

**Figure 9** XPS spectra of GO and rGO. (a-b) wide region: C1s, O1s peaks commonly appear, and N1s peak appear after reduction; (c-d) C1s region: Commonly 4 spectra related to graphitic C=C and functional groups (C-O, C=O, HO-C=O) appear in GO and rGO. Especially in rGO, additional peak with C-N appears.

**Figure 10** Change of rGO dispersion as pH conditions from 2 to 12. (a) Formation of agglomerate in rGO dispersion below pH 10, (b) Zeta potential of rGO dispersion as different pH; The most charged state is induced at pH 10.

**Figure 11** Photographs of rGO morphology change as varying pH (a) by stirring (SPH and SCH) after a while, and (b) waiting for natural self-assembly (WNH) after near 1 week.

**Figure 12** SEM images of rGO aerogels synthesized by method (1) among the three different approaches at each pH condition; rGO aerogels synthesized by pH control and a wait for natural self-assembly for hydrogel (WNH) (pH2, 4, 6, 8, 10, 12 in alphabetical order; every scale bar: 50  $\mu$ m); The morphology of rGO aerogels depend on pH conditions, indicating the dendrite-like structure is



shown below pH 10, the wire-like structure appears at pH10, the structure above pH10 is out of tendency.

**Figure 13** SEM images of rGO aerogels synthesized by method (2) among the three different approaches at each pH condition; rGO aerogel synthesized by stirring and extracting the supernatant by pipetting (SPH) (pH2, 4, 6, 8, 10, 12 in alphabetical order; every scale bar: 50  $\mu\text{m}$ ); The morphology of rGO aerogels depend on pH conditions, indicating the dendrite-like structure is shown below pH 10, the wire-like structure appears at pH10, the structure above pH10 is out of tendency.

**Figure 14** SEM images of rGO aerogels synthesized by method (3) among the three different approaches at each pH condition; rGO aerogels synthesized by stirring and extracting the supernatant by centrifuge for hydrogel (SCH) (pH2, 4, 6, 8, 10, 12 in alphabetical order; every scale bar: 50  $\mu\text{m}$ ); The morphology of rGO aerogels depend on pH conditions, indicating the dendrite-like structure is shown below pH 10, the wire-like structure appears at pH10, the structure above pH10 is out of tendency.

**Figure 15** Effect of salts in each rGO aerogel synthesized by (a) approach with pH control by stirring and separation by centrifuge (SCH), (b) approach with pH control by stirring and separation by pipette (SPH), and (c) approach with pH control and a wait for natural self-assembly (WNH). The salts noticeably appear in SPH and WNH, but hardly appear in SCH. The salts are pointed out with yellow arrows.

**Figure 16** (a-d) SEM images of rGO aerogel induced by stirring and centrifuge (SCH); (a-b) dendrite-like structure at pH2, (c-d) fiber-like structure at pH10.

**Figure 17** Raman spectra of rGO aerogels as changing pH; (a) D peak ( $\sim 1345\text{cm}^{-1}$ ) and G peak ( $\sim 1585\text{cm}^{-1}$ ) are similarly shown in each pH conditions, (b)  $I_D/I_G$  ratio and (c) position of both peaks as changing pH conditions. Entire data is not distinct from each other.

**Figure 18** Color change from yellow to black as controlling pH and reduction time: From left, GO at

pH3, pH10, rGO at pH 10 after 0.25h reduction, 0.5h reduction, 1h reduction, 1.5h reduction, 2h reduction. This is indicating the reduction is processed well.

**Figure 19** AFM images with (a) GO at pH3, (b) GO at pH10, and rGO after reduction with (c) 0.25h, (d) 0.5h, (e) 1h, (f) 1.5h, (g) 2h. (Every scale bar: 1 $\mu$ m) While GO sheets are isolated from each other due to functional groups on basal plane such as hydroxyl and epoxy groups, rGO sheets are overlapped because of reduction of functional groups on basal plane.

**Figure 20** UV-vis absorption spectra of GO and rGO. (a) UV-vis spectra of each graphene derivative, (b) Change of peak position after control of pH and reduction time. The peak of GO is red-shifted as reduction goes on, but the peak with GO is rather a little blue-shifted after pH control from 3 to 10.

**Figure 21** XPS analysis with GO and rGO; (a-b) Deconvoluted XPS spectra of GO at (a) pH3, (b) pH10; (c-g) Deconvoluted XPS spectra of rGO after (c) 0.25h, (d) 0.5h, (e) 1h, (f) 1.5h, (g) 2h reduction; (h) Change of C/O ratio as control of pH and reduction time; C/O ratio increases as reduction is processed, and after changing pH from 3 to 10.

**Figure 22** Raman analysis of GO and rGO. (a) Raman spectra of each graphene derivative. (b)  $I_D/I_G$  ratio after change of pH and reduction time. The positions of D and G peaks at each pH conditions are not differ from each other. While  $I_D/I_G$  ratio is increased as reduction is processed, it is decreased after changing pH condition from 3 to 10.

**Figure 23** Freezing-Thawing of GO and rGO. (a) Frozen rGO dispersion(left) and GO dispersion(right), (b) thawed rGO dispersion with agglomeration(left) which has agglomeration, and GO dispersion (right) which is completely re-dispersed, (c) SEM image of thawed rGO agglomeration, indicating scrolled structures are partially shown.

**Figure 24** SEM images of GO at (a) pH3, (b) pH10, and rGO at pH10 after (c) 0.25h, (d) 0.5h, (e) 1h, (f) 1.5h, (g) 2h reduction: All of Scale bars are 10 $\mu$ m. After changing pH condition, scrolled morphology is shown in common.

**Figure 25** TEM images of GNS, showing the scrolled state in GNS. This GNS is obtained from rGO aerogel at pH10 after 2h reduction.

**Figure 26** Dynamic light scattering (DLS) analysis of graphene derivatives: GO at (a) pH3, (b) pH10, and rGO at pH10 after (c) 0.25h, (d) 0.5h, (e) 1h, (f) 1.5h, (g) 2h reduction. (h) Change of diameter as variation in conditions with pH and reduction time. The size of GO or rGO sheets is remarkably decreased after pH change from 3 to 10, while the size is similar to each other in the other conditions.

**Figure 27** Zeta potential analysis of graphene derivatives with small sized GO sheets ( $\sim 1\mu\text{m}$ ) ; inset : comparison of Zeta potential between large sized GO ( $\sim 10\mu\text{m}$ ) and small sized GO ( $\sim 1\mu\text{m}$ ) at different pH. Zeta potential of large sized GO depends on pH conditions, but there is no outstanding change even after pH control and reduction.

## List of Schemes

**Scheme 1** Morphology and formation mechanism of porous graphene nanostructure depending on pH; Most of functional groups except for carboxyl groups on GO are reduced after hydrazine reduction, and this residual functional groups are crucial factor for the formation of different morphology depending on pH conditions.

**Scheme 2** Three approaches for synthesis of GNS; (a) Schematic of each procedure: In method 1, frozen rGO dispersion is under lyophilisation. And rGO film is obtained through filtration of thawed rGO dispersion including agglomeration in method 2. And thawed rGO dispersion is under re-freeze procedure and followed by lyophilisation in method 3; (b-d) SEM images of (b) GNS induced by method 1, (c) a film including GNS induced by method 2, (d) GNS induced by method 3.

**Scheme 3** Morphology and formation mechanism of GNS in polypropylene tube during Lyophilisation (Every scale bar: 50 $\mu$ m); While GNS is formed in the boundary of ice crystals, the stacked thick rGO structure is formed near the wall of polypropylene tube.

# Contents

|        |   |           |
|--------|---|-----------|
| 1.     | Introduction -----  | 1         |
| 1.1.   | Graphene synthesis -----  | 1         |
| 1.2.   | Various types of graphene nanostructures -----                          | 3         |
| 1.2.1. | Graphene thin films -----   | 3         |
| 1.2.2. | Porous graphene -----   | 4         |
| 1.2.3. | Graphene nanoscroll -----   | 6         |
| 2.     | Experimental -----  | 14        |
| 2.1.   | Synthesis of graphene oxide -----                                       | 14        |
| 2.2.   | Fabrication of graphene nanostructures -----                            | 15        |
| 2.2.1. | Graphene thin films -----   | 15        |
| 2.2.2. | Porous graphene -----   | 15        |
| 2.2.3. | Graphene nanoscroll -----   | 16        |
| 3.     | Results and Discussion -----  | 17        |
| 3.1.   | Characteristics of GO and reduced GO -----                              | 17        |
| 3.2.   | Porous graphene induced by pH control -----                             | 18        |
| 3.3.   | Graphene nanoscroll induced by pH and reduction -----                   | 20        |
| 3.3.1. | Characteristics of GO depending on pH and reduction time -----          | 20        |
| 3.3.2. | Morphology of graphene nanoscroll by control of pH and reduction time - | 21        |
| 4.     | Summary -----   | 46        |
| 5.     | Reference -----   | 47        |
|        | <b>Acknowledgement -----</b>  | <b>54</b> |

## 1. Introduction

In recent few decades, low dimensional carbon based materials have been widely researched. Especially, the discovery of monolayer graphene in 2004 has led to the demonstration of many novel properties in this versatile nanomaterial. Graphene is a flat monolayer of carbon atoms tightly packed into a two-dimensional (2D) hexagonal lattice, and is a basic building block for graphitic materials of all other dimensionalities (**Figure 1**). It can be wrapped up into 0D fullerenes, rolled into 1D carbon nanotubes (CNT) or stacked into 3D graphite.<sup>1</sup>

Graphene, the one-atom-thick planar sheets of sp<sup>2</sup>-bonded carbon atoms, shows intriguing physical, chemical and mechanical properties,<sup>1, 16, 17</sup> which include exceptional electron transport, large surface area, and excellent mechanical properties.<sup>18-20</sup> These unique properties and the distinct chemical composition of graphene distinguish it from other materials. Thus, graphene is the best candidate for a variety of applications with catalyst,<sup>21, 22</sup> sensor<sup>23-25</sup> and other energy fields etc.<sup>26-31</sup>

### 1.1. Graphene Synthesis

Geim and Novoselov exfoliated single layer graphene sheets using 3M tapes through physical approach.<sup>16</sup> Mechanical cleavage of graphite originally led to the discovery of graphene sheets and is the process currently used in most experimental studies of graphene. However, the low productivity of this method makes it unsuitable for large-scale use. For practical application, large quantity graphene must be synthesized. Chemical conversion from graphite is a much more efficient approach to bulk production of graphene sheets. So, many researchers have focused on the chemical approaches such as bottom-up and top-down method with different initial source. Typical bottom-up processes are chemical vapor deposition (CVD) of graphene on metal substrate and epitaxial growth of graphene on silicon carbide. Graphene from these methods has high quality for planar application, but it is unsuitable for 3D graphene based applications.<sup>22, 32, 33</sup>

In comparison, graphene from solution-processed bottom-up method could overcome this limitation. Moreover, there are additional advantages including (1) process with low cost, (2) needlessness of graphene transfer from the growth substrate, (3) affinity with other materials such as polymers, carbon-based materials, and nano particles.<sup>34</sup> First, relatively high quality graphene could be synthesized through graphite intercalate compounds (GIC), but it has also a problem with scale-up.<sup>35</sup> Graphene is also obtained by longitudinal unzipping of CNT.<sup>4, 36</sup> Generally, oxidation of graphite is widely used to get single layer graphene oxide which is a precursor of graphene. Graphene oxide was first synthesized in the nineteenth century,<sup>37, 38</sup> which means it has a longer history even than the

discovery of graphene. Graphene oxide has been prepared by the Brodie,<sup>38</sup> Staudenmaier<sup>39</sup> and Hummers<sup>40</sup> methods, and especially modified hummers method<sup>41-44</sup> is widely used up to now. After oxidation, graphene has functional groups on the surface, epoxy and hydroxyl groups on the basal plane and carboxyl acids along the edge.<sup>45</sup> These functional groups contribute to electrostatic repulsion between negatively charged graphene oxide sheets (**Figure 2**).<sup>2</sup> As a result, intrinsically hydrophobic graphene sheets change into hydrophilic, so graphene oxide sheets could be dispersed in aqueous solution.<sup>46</sup>

On the other hand, these functional groups also render graphene sheets insulated. However, this problem with conductivity could be partially resolved by reduction with chemical, thermal method. Even though reduced graphene oxide has more defect and lower conductivity than pristine graphene, this oxidation-reduction is facile method for versatile precursor of graphene-based materials in large-scale production (**Figure 3**).<sup>3</sup>

## 1.2. Various types of graphene nanostructures

As discussed in Section 1, graphene is the mother for other carbon-based materials. In addition, 2D graphene could be artificially modified with different morphology for various applications (**Figure 4**). Even though graphene itself is intriguing material, the fabrication of nanostructure with graphene could draw the enhanced distinct properties. Moreover, these graphene nanostructures could be a promising candidate for much more filed of application. So, the fabrication of graphene nanostructure renders significant advances to the materials science.

### 1.2.1. Graphene thin films

2D graphene sheets are synthesized various approaches such as CVD, epitaxial growth, mechanical exfoliation, and chemical oxidation-reduction. In this section, deposition with chemically synthesized graphene will be especially focused on. Generally, GO sheets are widely used for thin film because of solution-processibility than rGO sheets, and could be deposited on diverse substrates using methods such as drop-casting,<sup>47</sup> dip-coating,<sup>41</sup> spin-coating,<sup>48</sup> spraying,<sup>49, 50</sup> Langmuir-Blodgett,<sup>51-53</sup> and vacuum filtration<sup>31</sup> (**Figure 5**). After deposition, van der Waals interaction is attributed to strong adhesion of GO sheets on the substrate, and each sheet combines together with strong hydrogen bonding.<sup>31, 54</sup> This graphene thin film with GO sheets has advantages such as flexibility, mechanical stability, and tunability of electrical/optical properties.<sup>31</sup>

As mentioned above, graphene thin film is flexible, mechanically and stable, in addition, the electrical/optical properties of this film is tunable.<sup>31</sup> So, chemically modified graphene thin film is promising candidate for transparent conductors, sensors, thin film transistors, field emitters, photovoltaics, photo detectors etc.<sup>55</sup> Moreover, 3D porous graphene and GNS also are made up of this 2D graphene.

•



### 1.2.2. Porous graphene

Graphene has a tendency of irreversible aggregation or re-stacking because of van der Waals attractions and strong  $\pi$ - $\pi$  interaction. This aggregation or re-stacking of graphene sheets decreases the surface area, and consequently, the performance of electrochemical application is negatively influenced. Thus, it is important to prevent this re-stacking of graphene to obtain the large surface area. Considering this requirement, porous graphene structure is promising candidate for the aforementioned applications because of the tunability of nano porosities, thermal and chemical stability as well as its high specific surface area.<sup>56 57</sup>

There are several approaches for highly porous graphene structure using templates and hydrogel. Various templates have been used for porous graphene. For example, there are nano particles,<sup>8, 58</sup> bubble,<sup>9</sup> metal foam,<sup>11, 59</sup> CNT,<sup>10, 60</sup> and Oil drops<sup>12</sup>, etc. (**Figure 6**). Choi et al. reported porous graphene synthesized via PS templates for supercapacitors. 3D graphene frameworks with uniform macropore were synthesized using the PS colloidal particles.<sup>58</sup> And Xiao et al. reported hierarchically porous graphene structure using bubble template. Their structure had nanoscale pores as well as micropore channels.<sup>9</sup> Moreover, Chen et al. presented 3D flexible and conductive interconnected graphene networks using Ni foam as a template.<sup>59</sup>

Even though these method using templates is efficient for porous graphene structure, it is unavoidable to etch the template through the additional process. Hence, monolith porous graphene structure has been synthesized through graphene hydrogel. Xu et al. suggested a one-step hydrothermal process for graphene hydrogel. This hydrogel can be converted to porous structure by lyophilisation.<sup>61</sup> Other researchers also presented self-assembly process for porous structures-supported nano particle like  $\text{Fe}_3\text{O}_4$ . This  $\text{Fe}_3\text{O}_4$  is one of the nano particles which are efficient at lithium ion insertion and extraction. So, these porous structures are promising candidates for electrode of rechargeable lithium-ion batteries.<sup>62-64</sup>

As mentioned earlier, porous graphene structure has large surface area as well as intrinsic exceptional physical and chemical properties. Tremendous attention and research of this porous graphene structure are attributed its distinction, and this structure has been widely applied in the various fields such as energy storage, sensor, catalyst, pollutant absorbents etc.

In the field of energy storage, monolithic porous rGO structure was directly used as an electrode material for supercapacitors. Large accessible surface of this porous rGO structure could give facile routes for electron and electrolyte transportations in interconnected conductive network. As a result, nearly 50% higher specific capacitance of  $152\text{Fg}^{-1}$  was evaluated, as compared with the result from supercapacitors using rGO agglomerate particles at the same conditions ( $100\text{Fg}^{-1}$  at scan rate of

20mVs<sup>-1</sup>).<sup>61</sup> On the other hand, porous rGO was also utilized as buffered materials which could support SnO<sub>2</sub> particles, an excellent anode material for Li-ion batteries (LIBs), during charge/discharge process. Consequently, cyclic performance of these LIBs could be improved using enough void spaces of porous structure owing to the prevention of breakdown induced from lithium insertion.<sup>65</sup>

Additionally, porous graphene structure could be used for high sensitivity detection of environmental pollution gases such as NH<sub>3</sub>, NO<sub>2</sub> in the ppm range.<sup>66</sup> This sensor with porous graphene showed higher sensitivity compared with individual SWNT device<sup>67</sup> and commercially available conducting polymer sensors.<sup>68</sup> Furthermore, large surface of porous graphene structure contributes the efficient pollutant absorption. It could be used to remove heavy ions and oils in the field of water purification.<sup>63</sup>

Consequently, although many researches have proposed diverse approaches for porous graphene structure, there are still several problems to solve. As mentioned above, additional process is necessary to remove the templates which are used to make pores. And tough conditions with high temperature and pressure are needed in case of hydrothermal process. Moreover, it is difficult to control the porosity of structure. In addition, this porous graphene is promising material for the field of various applications. Therefore, the facile fabrication for porous graphene has been still widely explored.

### 1.2.3. Graphene Nanoscroll

In general, graphene (2D), carbon nanotube (1D), and fullerene (0D) are known as the typical carbon-based materials, and these materials have widely explored owing to their noticeable properties. Recently, another intriguing carbon-based material, which is graphene nanoscroll (GNS), is focused on. This material is one of the derivatives from 2D graphene, while the morphology is similar to 1D carbon nanotube (CNT). Hence, GNS, which is hybrid of graphene and CNT, is expected to have some distinct characteristics such as electronic<sup>69</sup> and optical properties<sup>70</sup> unlike graphene and CNT<sup>14, 15</sup>

This fascinating material was first fascinated using arc-discharge by Bacon in 1960.<sup>71</sup> And recently several approaches have been developed for GNS, with high energy ball milling of graphite,<sup>72</sup> microwave spark assistance in liquid nitrogen,<sup>14</sup> and chemical methods.<sup>13, 15, 73-76</sup> Especially, many researchers have tried with various chemical routes. Viculis et al. reported the chemical route for carbon nanoscroll using exfoliation and sonication process. They considered that sonochemical energy is the key to forming GNS.<sup>13</sup> Similarly, Zeng et al. demonstrated sonication process is important process for formation of GNS, and they also used graphite intercalation compounds (GICs) with  $KC_8$ .<sup>73, 74</sup> Shioyama and coworker also synthesized GNS using GIC and sonication.<sup>75</sup> This chemical route using GIC and sonication is the most efficient but a drawback with impurity and defects exist. Additionally, Zhou et al. produced GNS through  $CO_3O_4$  scroll with assistance of surfactant.<sup>77</sup> And Xie et al. introduced another process with mechanical exfoliation using isopropyl alcohol (IPA) solution,<sup>15</sup> but, this method has a limitation with low yield. Various approaches for GNS have been widely explored, but the facile method is still needed to achieve the high quality, purity with high yield in safe conditions (**Figure 7**).

Unlike CNT, the diameter of GNS is tunable through the chemical doping because GNS has open-edge.<sup>5</sup> Owing to these unusual properties, GNS have been focused on as potential materials for nano actuators and nano mechanical devices.<sup>5</sup> In addition, GNS could facilitate for energy materials such as supercapacitors<sup>74, 76</sup>, batteries<sup>13</sup>, and hydrogen storage<sup>78, 79</sup>.

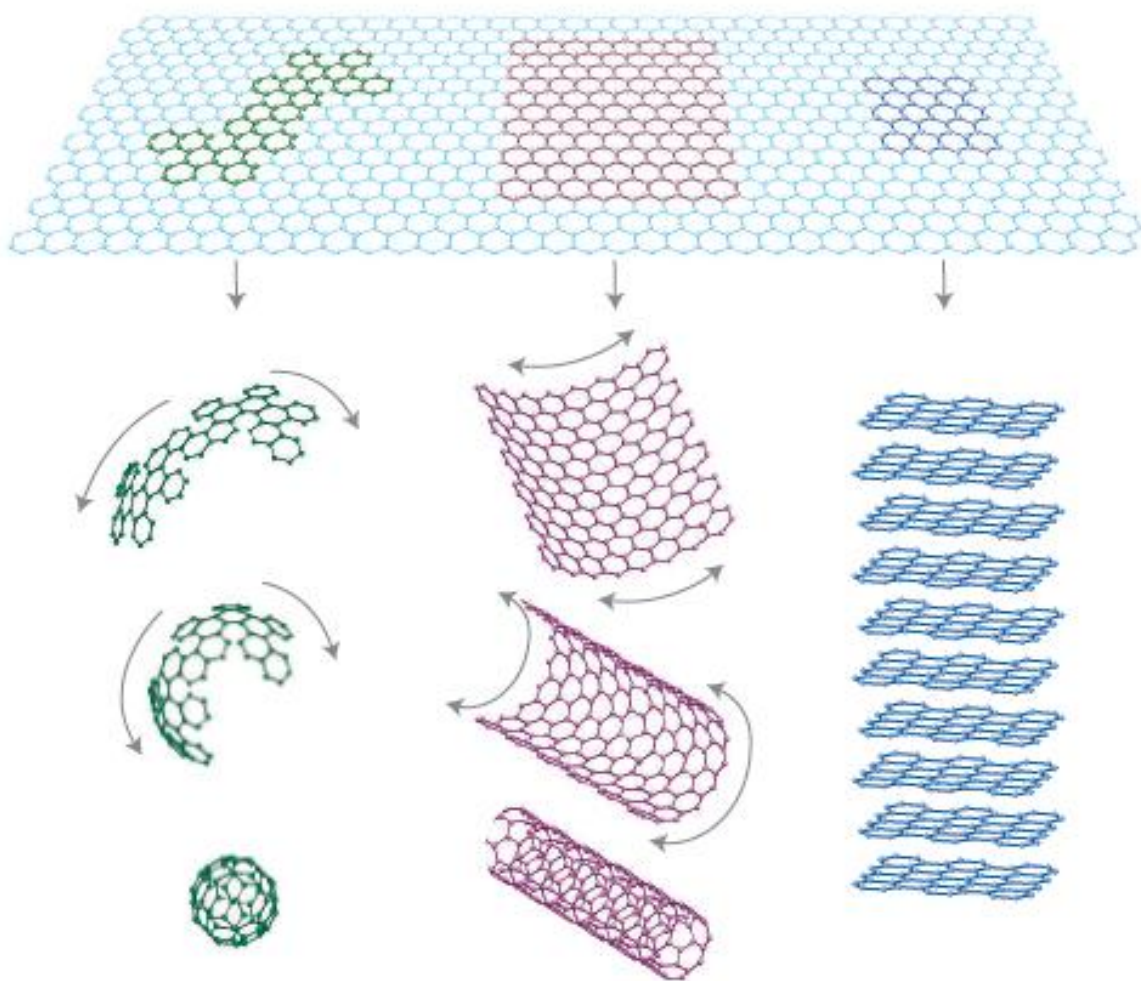


**Figure 1** Carbon-based materials modified with a graphene sheet as a 2D basic building block; Fullerene (0D), Carbon Nanotube (1D), Graphite (3D)<sup>1</sup> (Geim and Novoselov, *Nat. Mater.* **2007**, 6, 183)

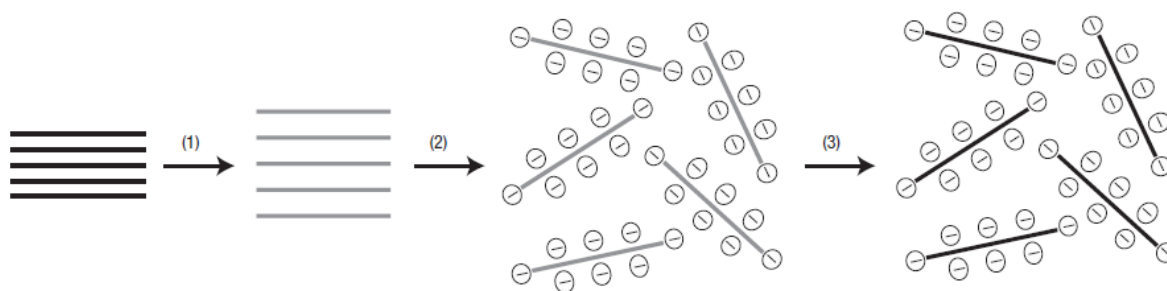


**Figure 2** Chemical approach of aqueous graphene dispersion. (1) Oxidation of graphite to graphite oxide with increased interlayer distance. (2) Exfoliation of graphite oxide in aqueous solution by sonication to obtain GO colloids which are stabilized by electrostatic repulsion. (3) Controlled conversion of GO colloids to conducting graphene colloids through chemical reduction using hydrazine.<sup>2</sup> (Li et al., *Nat. Nanotechnol.* **2008**, 3, 101)

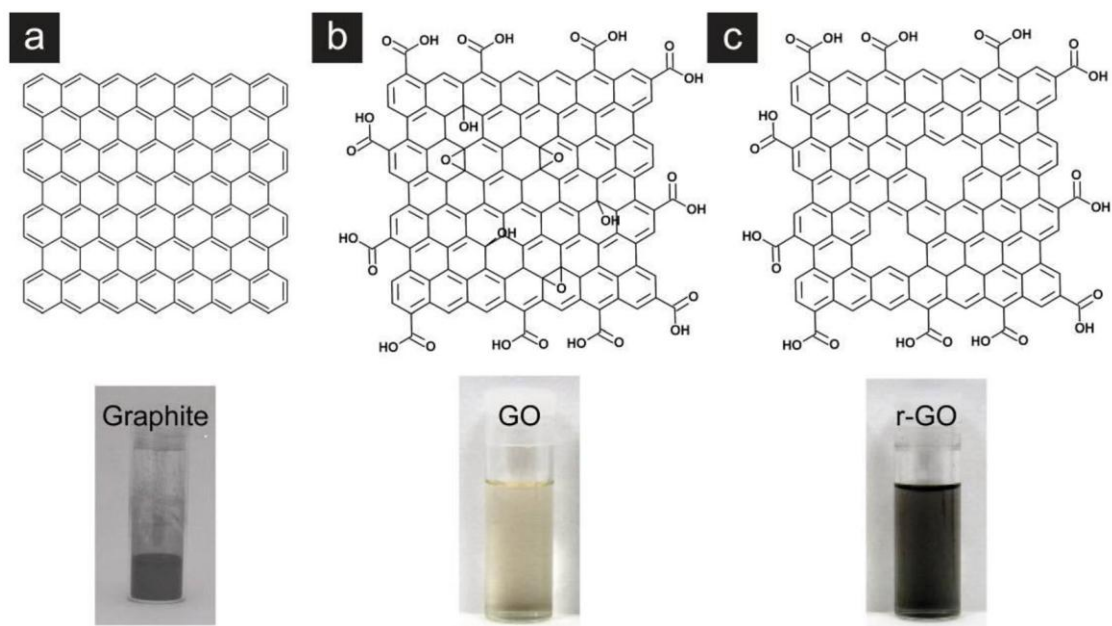


**Figure 3** Structure of graphene derivatives synthesized by oxidation and reduction.<sup>3</sup> (Cote et al., *Pure Appl. Chem.* **2011**, 83, 95)

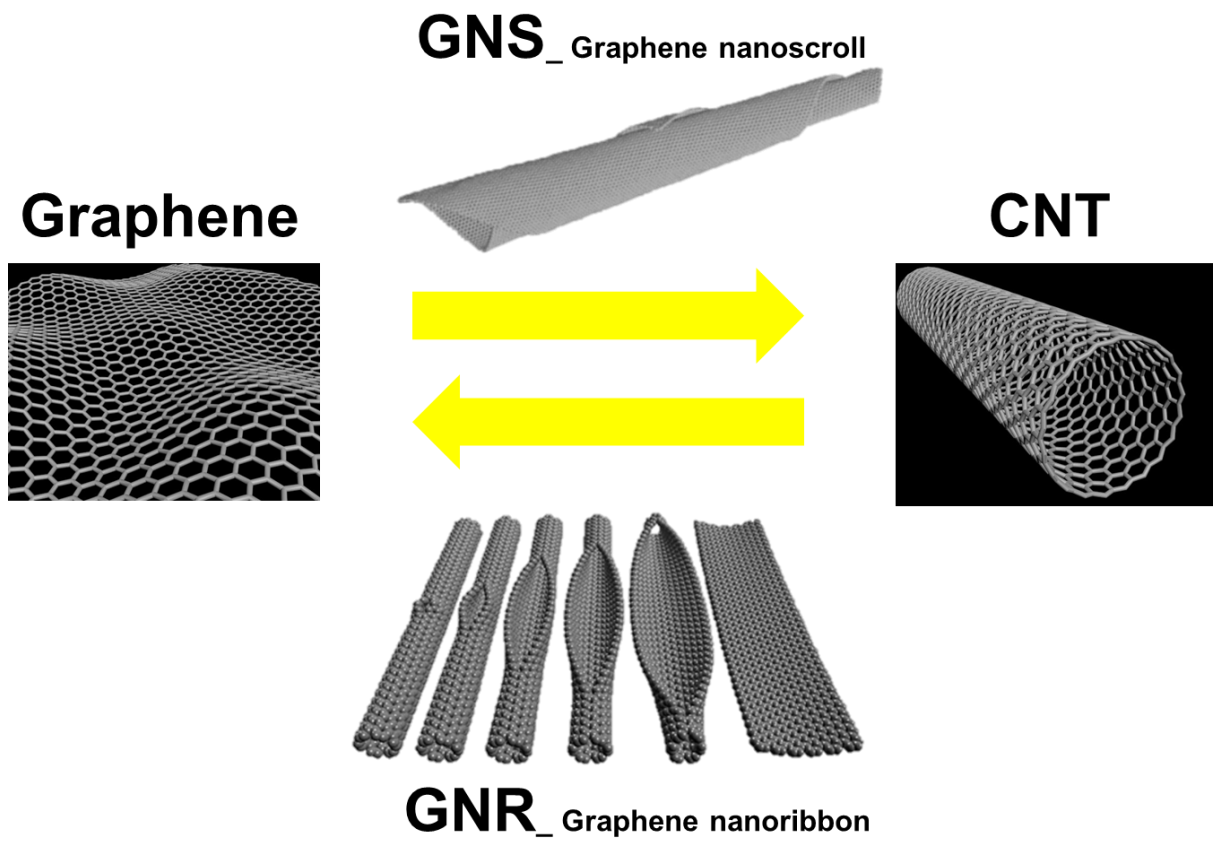


**Figure 4** Different morphology of carbon-based materials such as graphene, CNT, graphene nano scroll (GNS)<sup>5</sup>, graphene nano ribbon<sup>4</sup>. (Kosynkin et al., *Nature* **2009**, 458, 872; Braga et al., *Nano Lett.* **2004**, 4, 881)

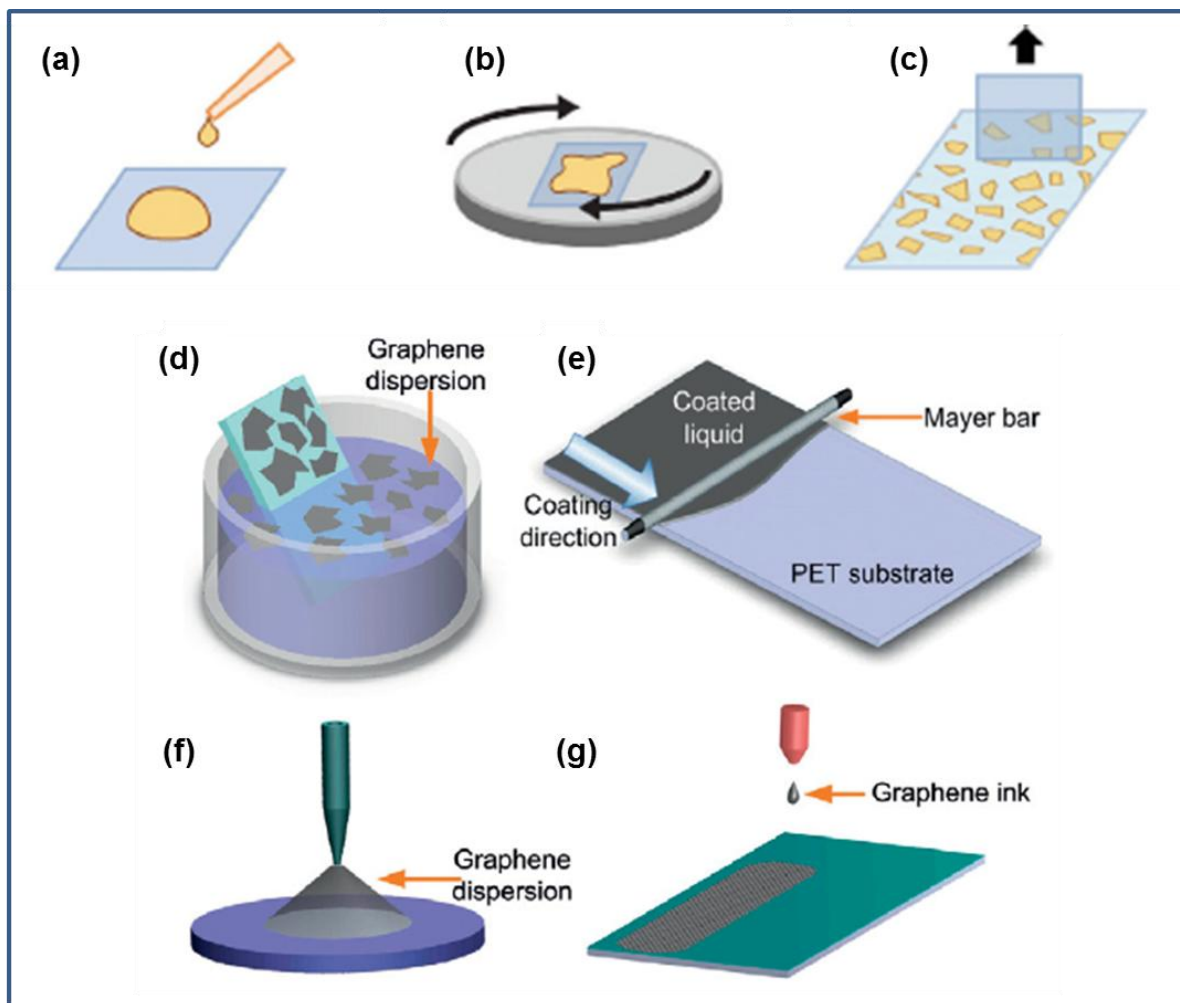


**Figure 5** Fabrications for graphene thin films; (a) drop casting, (b) spin coating, (c) Langmuir-Blodgett assembly,<sup>6</sup> (d) dip casting, (e) rod coating, (f) spray coating, (g) inkjet printing.<sup>7</sup> (Kim et al., *Materials today*, **2010**, 13, 28; Bonaccorso et al., *Materials today*, **2012**, 15, 564)



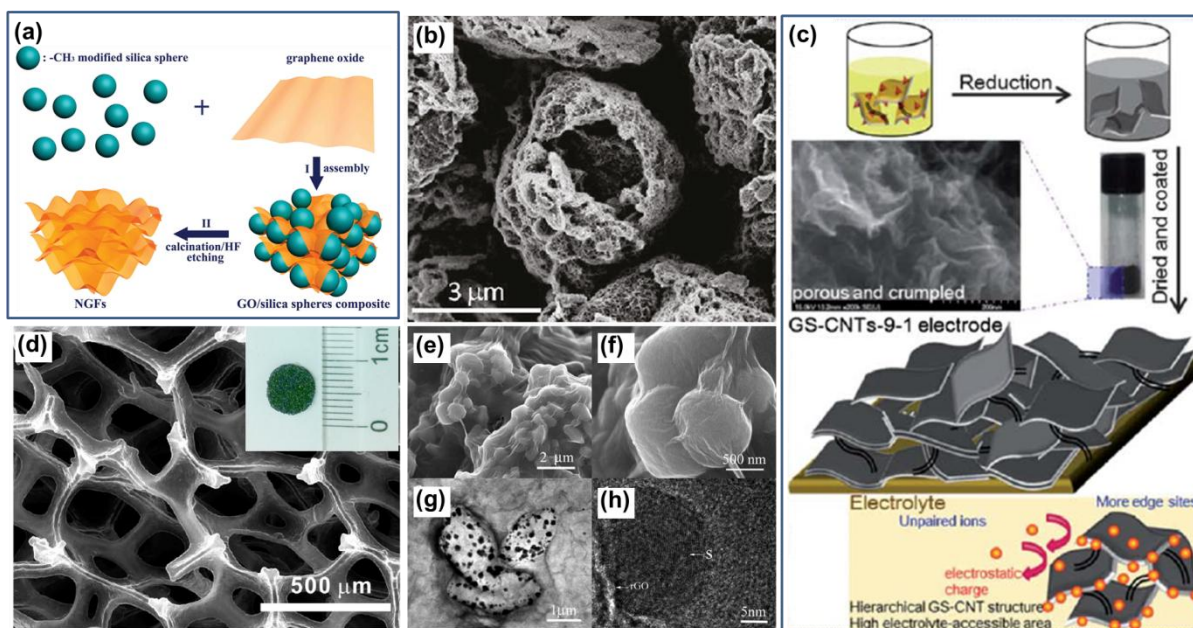


**Figure 6** Various approaches for porous graphene structures. (a) Schematic illustration of the synthesis procedures of the porous graphene foams using silica templates<sup>8</sup> (Huang et al., *Adv. Mater.* **2012**, 24, 4419), (b) SEM image of hierarchically porous graphene structure using bubble templates<sup>9</sup> (Xiao et al., *Nano Lett.* **2011**, 11, 5071), (c) Schematic procedures of preparing graphene sheets-CNTs electrode<sup>10</sup> (Yang et al., *J. Mater. Chem.* **2011**, 21, 2374), (d) SEM image of the ultrathin graphite foam with micropores; inset: photograph of this foam<sup>11</sup> (Ji et al., *Nano Lett.* **2012**, 12, 2446), (e-h) Morphology of rGO encapsulated sulfur synthesized via oil-water system, (e-f) SEM, (g) TEM, and (h) HRTEM images of this porous structure<sup>12</sup> (Zhang et al., *J. Mater. Chem.* **2012**, 22, 11452).

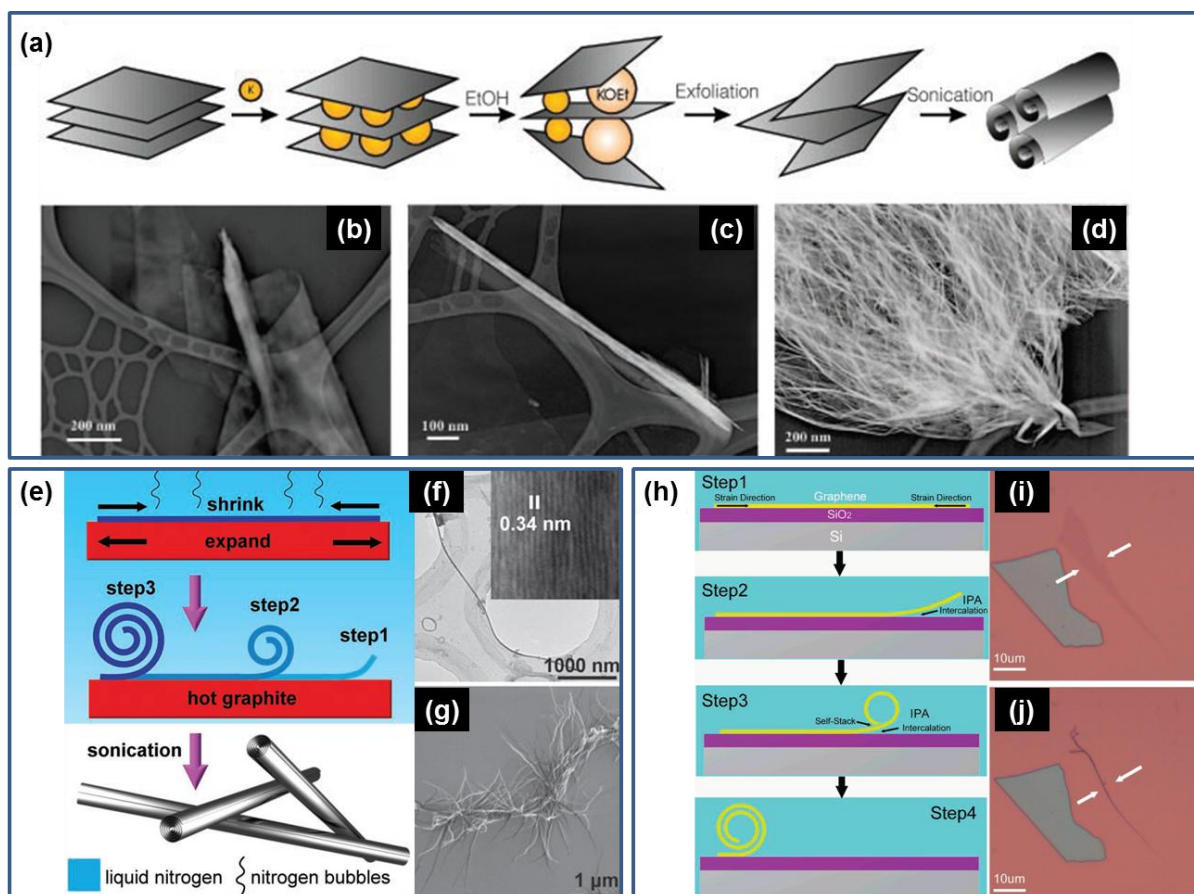


**Figure 7** Graphene nanoscroll (GNS) with various approaches; (a) Chemical route for GNS with exfoliation/sonication process and (b-d) TEM images of GNS<sup>13</sup> (Viculis et al., *Science* **2003**, 299, 1361); (e) Microwave spark assistance in liquid nitrogen for GNS, (f-g) TEM and SEM images with GNS<sup>14</sup> (Zheng et al., *Adv. Mater.* **2011**, 23, 2460); (h) Mechanical exfoliation using isopropyl alcohol (IPA) for GNS, (i-j) Optical microscope images of (i) graphene sheet and (j) scrolled graphene sheet<sup>15</sup> (Xie et al., *Nano Lett.* **2009**, 9, 2565).

## 2. Experimental

### 2.1. Synthesis of graphene oxide

Graphene oxide was prepared using modified hummers method.<sup>43,44</sup> In brief, graphite powder (SP-1, Bay Carbon),  $K_2S_2O_8$  (Sigma Aldrich), and  $P_2O_5$  (Sigma Aldrich) were added to concentrated  $H_2SO_4$  (Sigma Aldrich). This solution was heated using  $80^\circ C$  oil bath for 4.5 hours with vigorous stirring. Then, the solution was carefully diluted with de-ionized water, followed by vacuum filtration with additional DI washing to make the pH neutral. The filtrate was dried in a  $30^\circ C$  vacuum oven overnight. The pre-oxidized graphite was then added to concentrated  $H_2SO_4$  in an ice bath. And then,  $KMnO_4$  (Sigma Aldrich) was slowly added with vigorous stirring, being careful not to exceed  $20^\circ C$ . The solution was moved from the oil bath into a  $36^\circ C$  bath and heated for 2 hours. Then, the mixture was gradually diluted using DI water in an ice bath, being careful not to exceed  $50^\circ C$ . Next, the mixture was heated using a  $35^\circ C$  bath for 2 hours, followed by additional dilution with much more DI water to terminate the reaction. After that, 30%  $H_2O_2$  (Sigma Aldrich) was added to this mixture, which process changed the color into bright yellow with violent bubbles. This mixture was stirred for 0.5 hour and followed by centrifugation several times with 10% HCl to remove residual salts. And then this solution was subjected to dialysis to adjust the acidity. The result solution was concentrated and dried in vacuum oven at  $30^\circ C$ . Finally, dried GO is achieved after few days drying.

## 2.2. Fabrication of graphene nanostructures

### 2.2.1. Graphene thin films

GO solution was achieved by re-dispersion of the dried one in DI water by sonication. And these GO sheets in solution were coated on Si wafer by spin coating or drop casting. Meanwhile, when the rGO sheets are needed, additional reduction process is necessary. For solution-processed procedure, GO was reduced by chemical approach, especially using hydrazine monohydrate (35wt% in water, Sigma Aldrich) which is an effective reducing agent.<sup>2</sup>

The obtained brown graphene oxide solution was centrifuged with 4000rpm for 10min to remove any unexfoliated graphite oxide. Then, hydrazine monohydrate and ammonia solution (28wt% in water) were added to the graphene oxide solution. The suspension of GO with relatively low concentration (0.5mg/ml) was used to obtain graphene thin film through the coating procedure.<sup>55</sup> And especially, ammonia solution was introduced until the graphene oxide solution was adjusted into pH10. This mixture was heated at 90°C for 2 hours, and the color of solution changed to black as the reduction occurred.<sup>2</sup> The rGO sheets were likewise coated on Si wafer by several coating methods.

### 2.2.2. Porous graphene

As mentioned in section1.2.2, porous nanostructure with graphene is fabricated using various templates such as nano particles,<sup>8, 58</sup> bubble,<sup>9</sup> metal foam,<sup>11, 59</sup> CNT,<sup>10, 60</sup> and Oil drops<sup>12</sup>, etc. Meanwhile, hydrothermal approach is also used to fabricate the monolithic porous graphene without any templates<sup>61-64</sup>, indicating the procedure for removal of templates is unnecessary. Even though this hydrothermal method is facile approach for fabrication of porous graphene, critical conditions with high pressure and high temperature are needed to use this method. Hence, we fabricated porous graphene with facile approach which is depending on only pH control in mild conditions.

The porous structure was prepared using pH control and lyophilisation with fully reduced graphene oxide (rGO). The rGO dispersion was adjusted from pH2 to pH12 using HCl and NH<sub>4</sub>OH. And rGO agglomeration in dispersion was induced by three approaches. (1) The pH-adjusted solution was left to separate rGO agglomeration from dispersion naturally. It takes from few days to a week depending on the amount of hydrogel. And then, the supernatant except rGO agglomeration in separated solution was removed. This method was named 'WNH (wait for natural self-assembly for hydrogel)'. (2) When the acid drop was introduced into rGO dispersion, the pH-adjusted solution was simultaneously stirred to render rGO dispersion unstable. Just as soon as the acid droplet was mixed, agglomeration

appeared in rGO solution. And this suspended agglomeration gradually sank after a while. This result hydrogel was obtained after removing the supernatant by pipetting. And this second method was named 'SPH (Stir and extract the supernatant by pipetting for hydrogel)'. (3) Third method started from synthesis the rGO agglomeration by second method. And then, it was subjected to centrifugation and followed by removing the supernatant. This method was named 'SCH (stir and extract the supernatant by centrifuge for hydrogel)'.

### 2.2.3. Graphene nanoscroll

Generally, the traditional research with GNS has focused on theoretical approaches with simulation.<sup>5, 69, 70, 78-82</sup> And the facile production in safe conditions is still absent in spite of various methods for the fabrication of GNS have been widely explored.<sup>13-15, 72-76, 83</sup> So, we fabricate the facile method for GNS in safe conditions.

First, GO dispersion with acidic condition (initial state) and with base condition are prepared. The latter is adjusted using  $\text{NH}_4\text{OH}$  as stated in section 2.2.1. And then, while it is in reduction progress, a certain amount of dispersion was extracted from the reactor at each moment (0.25h, 0.5h, 1h, 1.5h, 2h) and followed by natural cooling. The result solution with different reduction time was converted into chemically modified graphene aerogel through lyophilisation. And this process is more minutely described in **Scheme 2** which shows the processing for aerogel- or film-type samples with three different methods. Method 1 is primary approach for aerogel-type samples, while thawing process was added in method 2 and 3. In method 2, the frozen graphene dispersion which is the result one before lyophilisation in method1 is thawed naturally, and followed by filtration using polycarbonate membrane with  $0.2\mu\text{m}$ . And then, this filtrated film is dried in  $30^\circ\text{C}$  vacuum oven. Similarly, in method 3, the frozen graphene dispersion in method1 is thawed naturally, and followed by re-freezing to confirm whether the effect of freezing process exists or not.

### 3. Results and Discussion

#### 3.1. Characteristics of GO and reduced GO

GO which we used was prepared by modified Hummer's method. The dimension and thickness of this GO were  $1\mu\text{m}$  and below  $1\text{nm}$ , which were characterized by AFM (**Figure 8a**), indicating presence of functional groups on basal plane of GO. This GO dispersion was reduced using hydrazine to restore the inherent properties, and this difference between GO and rGO was monitored by UV-vis absorption spectra, Raman spectra, and XPS.

First, absorption peak of GO dispersion at  $231\text{ nm}$  is red-shifted to  $270\text{nm}$  after reduction in UV-vis absorption spectra (**Figure 8b**). This phenomenon is attributed to lengthened conjugation, indicating the restoration of  $\text{sp}^2$  structure.<sup>2</sup> In Raman spectra, GO had G peak at  $1350\text{cm}^{-1}$  and D peak at  $1580\text{cm}^{-1}$  and the ratio of D to G increased as reduction (**Figure 8c**). This phenomenon could occur when the average size of the  $\text{sp}^2$  domains decreases after reduction, indicating the size of newly created domains after reduction are smaller than the size of GO before reduction.<sup>84, 85</sup> However, further research with the change of  $I_D/I_G$  ratio is required because this is still controversial.<sup>55</sup>

XPS was used to analyze the GO and rGO using Al  $K\alpha$  source. **Figure 3** presents the C1s XPS spectra of GO and rGO with wide region and C1s region. The C/O ratio was remarkably increased and additional N1s peak appeared after reduction (**Figure 9a-b**). The C1s XPS spectrum of GO (**Figure 9c**) indicated the degree of oxidation with four components which correspond to C atoms in different functional groups. The non-oxygenated ring C=C appeared at  $284.31\text{eV}$ , the C atom in C-O bond at  $286.28\text{eV}$ , the carbonyl C (C=O) at  $288.09\text{eV}$  and the carboxylate carbon (HO-C=O) at  $289.38\text{eV}$ . The C1s XPS spectrum of rGO (**Figure 9d**) also had these same functional groups, but the peaks shifted a little and the intensities were decreased. Unlike most of peaks, the peak at  $284.21\text{eV}$  indicating the C=C bond increased after reduction. And additional peak appeared at  $285.48\text{eV}$  corresponding to the C=N bond, which is caused by chemical reduction using hydrazine. Consequently, this result supports the traditional research, indicating that hydrazine reduction is ineffective for removal of carboxyl groups on GO<sup>2, 55, 85-87</sup> and has the n-doping effect<sup>85, 88-90</sup> because of additional peak related to C-N after reduction.

### 3.2. Porous graphene induced by pH control

We explored a readily accessible and inexpensive approach for porous graphene structure using pH control and lyophilisation. Graphene sheets were crumpled each other at low pH while they were rolled up at high pH (**Scheme 1**).

Unlike GO sheets, it is hard to disperse rGO sheets in aqueous solution without any surfactant because rGO sheets tend to agglomerate together with a decrease of functional groups. However, rGO could be also dispersed well in aqueous solution at high pH since carboxylic groups at the edge of rGO sheets remain even after reduction. Because reduction using hydrazine could not reduce the carboxylic groups on GO sheets.<sup>91</sup> In high pH solution, deprotonated carboxylic groups on rGO sheets render that dispersible in aqueous solution. Hence, rGO sheets were dispersed well at high pH, while they were crumpled each other and formed hydrogel at low pH (**Figure 10 a**).

In addition, Zeta potential of rGO dispersion also shows this tendency, indicating the stability of rGO dispersion is sensitive to pH change. GO sheets have lots of functional groups like epoxide, hydroxyl group at the basal planes and carboxyl group at the edges, and these functional groups make GO sheets suspensible in aqueous solution.<sup>92</sup> Most of functional groups are removed after chemical reduction with hydrazine, but carboxyl groups are unlikely to be removed as mentioned above. So, these remaining carboxyl groups at the edges of rGO sheets are important key to disperse rGO sheets in aqueous solution.<sup>2</sup> **Figure 10b** shows that the Zeta potential of rGO depending on pH, and rGO sheets at pH10 were most stable in solution with the highest Zeta potential. Carboxyl groups at the edges of rGO sheets are deprotonated in high pH condition, which makes rGO sheets more negatively charged and electrostatic repulsion among rGO sheets becomes stronger. As a result, rGO sheets could be stable even after reduction. However, over pH10, the potential of rGO dispersion increased, which means it is rather less stable. This decreased stability of rGO at pH above 10 results from the compression of the double layer at high ionic strengths.<sup>91</sup>

With this stability of rGO sheets in aqueous solution as varying pH value, several approaches were used for synthesis of hydrogel. First, the hydrogel was formed by self-assembly after diffusion of few acid drops into rGO dispersion. It takes from few days to a week depending on the amount of hydrogel (WNH). Second, the hydrogel was generated by stirring after introducing few acid drops into rGO dispersion. And the supernatant except for hydrogel was extracted by pipette (SPH). Third, the hydrogel which was made by second approach was obtained after centrifuge to remove the supernatant (SCH). The similar tendency was appeared as pH control in each approach (**Figure 11**).

In the case of WNH, hydrogel was spontaneously formed at low pH after several days, which it took time to diffuse a drop of acid solution. Even though the SEM images present the tendency of

rGO morphology as pH change (**Figure 12a-f**), this network in the hydrogel was easy to collapse and there was a lack of reproducibility as well as the problem with salt generation. In comparison, it is simple to stir the dispersion for the formation of hydrogel and extract the supernatant by pipette (SPH). Moreover, this method also had a tendency of rGO morphology as pH change (**Figure 13a-f**). But, this approach also had a problem with salts in result aerogel. Hence, we separated the supernatant from hydrogel by centrifuge and followed by extraction (SCH). This method also presents the tendency of rGO morphology as pH change (**Figure 14a-f**), indicating the rGO structure is irregularly connected at low pH while the rGO sheets are rolled up at high pH, especially pH 10. And rGO aerogel at pH12 was also out of tendency like the result of Zeta potential analysis. And the amount of salts in the rGO aerogel was remarkably decreased when using centrifuge approach (**Figure 15**).

After formation of hydrogel, it was processed by lyophilisation. **Figure 16 a-d** presents SEM images of the morphology difference between rGO structures at pH2 and pH10. The rGO sheets were connected each other and then formed dendrite-like structure at pH2 (**Figure 16 a-b**). Meanwhile, rGO sheets were rolled up and resulted in wire-like structure at pH10 (**Figure 16 c-d**). This tendency is caused from the stability of rGO sheets in aqueous solution. The crumpled rGO at pH2 could be formed before lyophilisation, and this structure remained even after lyophilisation. Whereas, it is surmised that well-dispersed rGO sheets at pH10 have a tendency to be rolled up during freezing and this rolled structure also remained after drying. This phenomenon might be affected by formation of ice. Qiu et al. showed that the honey comb structure is formed in high concentrated rGO conditions during lyophilisation, and they also explained that the rolled structure appeared in low concentrated rGO conditions.<sup>93</sup> This phenomenon will be minutely discussed in next section. Additionally, Raman spectra of every pH condition have D peak and G peak (**Figure 17**). As increasing pH, both D and G peaks had a tendency to blue-shift a little, even though there was not any other noticeable  $I_D/I_G$  ratio change as varying pH.

Entirely, the formation of pH-dependent porous graphene structure is attributed to the chemistry of modified graphene, indicating the residual functional group, carboxyl group, on rGO even after reduction is crucial factor to control the porous graphene structure. As a result, this method could be readily used without the critical conditions such as the use of templates and hydrothermal approach contrary to other traditional researches which are mentioned above.



### 3.3. Graphene nanoscroll induced by pH and reduction

#### 3.3.1. Characteristics of GO depending on pH and reduction time

As discussed above, wire-like morphology of rGO was appeared at pH10 condition, and this structure has been called graphene nanoscroll (GNS). In this section, we fabricate an interpretation of the formation of GNS. We assumed that scrolled phenomenon is attributed to the change of chemistry of modified graphene during pH control and reduction. So, rGO dispersion depending on reduction time was used. Since rGO sheets tend to agglomerate during reduction procedure without the procedure of pH adjustment into alkaline, it is hard to fabricate GNS with these crumpled rGO sheets.<sup>2</sup> Thus, rGO dispersion we used was induced at pH10 before reduction for the stability in aqueous solution. Given the possibility of chemistry change after pH adjustment from acid into alkaline, pH control is also necessary to understand the mechanism of GNS formation. So, GO dispersion with different pH, 3 and 10, were also used in this research. **Figure 18** shows the color change depending on pH and reduction time. The color of GO dispersion changed from yellow into black, which means the reduction gradually processed. Unexpectedly, difference of pH also affected the color change of GO dispersion.

The size of GO sheets used in this research was nearly 1 $\mu$ m, which are characterized by AFM (**Figure 19**). While GO sheets are isolated from each other, rGO sheets are partially overlapped as the reduction progresses. This overlap is attributed to  $\pi$ - $\pi$  interaction that arises from restoration of sp<sup>2</sup> conjugation after reduction. The procedure of reduction could be also monitored through the UV-vis spectroscopy. As shown in **Figure 20**, the peak of GO gradually redshifts from nearly 230nm to above 260nm as reduction goes on. This phenomenon is caused from lengthened conjugation, indicating the restoration of sp<sup>2</sup> structure<sup>2</sup> as mentioned in section 3.1.

Furthermore, XPS also shows the progress of reduction with different ratio of deconvoluted peaks as reduction goes on (**Figure 21**). As explained above, we could monitor the gradually decreased peaks with C-O, C=O, HO-C=O, while the peak of C-N appears as the reduction goes on. Overall, C/O ratio is increased after control of pH and reduction time, which also demonstrates the restoration of original sp<sup>2</sup> conjugation.

**Figure 22** represents Raman spectra of GO and rGO in each condition. Except the change of I<sub>D</sub>/I<sub>G</sub> ratio, any noticeable difference of each peak is absent (**Figure 22a**). The pH effect is also appears in the Raman spectra, which I<sub>D</sub>/I<sub>G</sub> ratio is decreased after adjusting the pH from 3 to 10 (**Figure 22b**).

### 3.3.2. Morphology of graphene nanoscroll by control of pH and reduction time

In the section 3.2.1, the characteristic of GO was affected by pH as well as reduction time. Even though this phenomenon is still uncertain, we monitored the morphology change from this effect. To investigate the procedure of GNS formation, three different methods were used (**Scheme 2a**). Method 1 is major approach for aerogel-type samples, while method 2 is for film-type samples. And method 3 is to confirm when GNS is formed.

Consequently, diverse morphologies of rGO were appeared, as shown in **Scheme 2b-d**. **Scheme 2b** presents the morphology of GNS, and the film in **Scheme 2c** has no porous structure partially even with GNS, while GNS which is unscrolled a little is appeared even after re-freezing in **Scheme 2d**. Entire SEM analysis indicates that the film-type of GNS was not readily constructed contrary to expectations, and it was surmised that GNS was formed during freezing process. To ensure this assumption with formation of GNS, the morphology of rGO agglomeration which was appeared after re-freezing was verified by SEM right after thawing process (**Figure 23**). Through this analysis, it could be surmised that GNS are already formed during not lyophilisation, but freezing procedure.

To confirm the cause of this formation, the morphology of each rGO with different reduction time and GO with different pH were also monitored. Unexpectedly, GNS are appeared in every rGO with different reduction time and the morphology difference exists between GO in basic conditions and acidic conditions (**Figure 24**). Unlike GO at pH10 has GNS, there crumpled structure in GO at pH3, and GNS is also characterized by TEM (**Figure 25**).

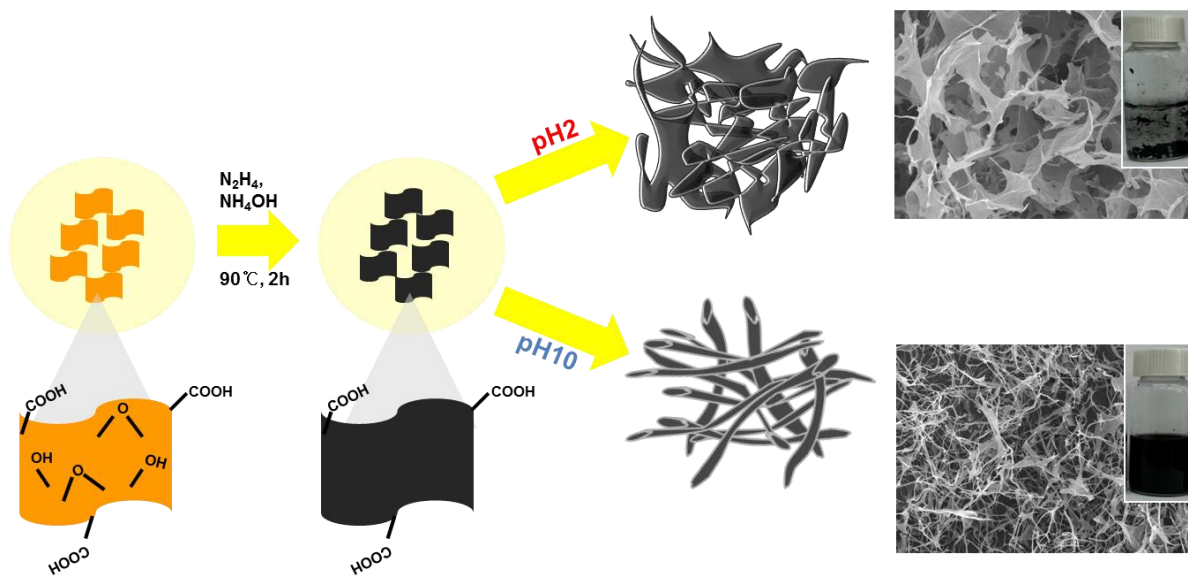
**Scheme 3** presents the mechanism of GNS formation during freezing process, and the morphology in the different positions which are a wall of polypropylene tube and the boundary of ice crystals. During freezing process, rGO sheets are stacked near the wall of tube which is hydrophobic, while rGO sheets in the boundary of ice crystals are spontaneously scrolled to enhance the stability. Even though Qiu et al. presented the cork-like graphene monolith using ice crystals as templates, our result structure was not regularly connected each other. This result is attributed to different concentration and size of GO. Since the concentration of their GO dispersion (5mg/ml) is 10 times of ours (0.5mg/ml) and the difference of GO size also exists.<sup>93</sup> So, GNRs are shown in our case unlike their case.

Once both ends of a rGO sheet start to overlap, formation of GNS is attributed to van der Waals interaction.<sup>5</sup> And, Viculis et al. demonstrated graphene sheets scroll during sonication, which is

induced by additional sonochemical energy.<sup>13</sup> Hence, more certain evidences are needed to investigate the formation of GNS. So, dynamic light scattering (DLS) was used to monitor the state of GO and rGO sheets in dispersion. **Figure 26** presents that the size of GO sheets are sharply decreased as changing the condition of pH, while the size of rGO sheets have no remarkable change as reduction goes on. It is surmised that rGO sheets are already scrolled from when pH is adjusted from 3 into 10 and GNS are more scrolled under van der Waals interaction as reduction progresses.

To obtain the additional evidence, the charge state in dispersion was monitored by Zeta potential (**Figure 27**). However, each Zeta potential of dispersion with different conditions has no remarkable change contrary to our expectation, all of dispersion shows highly negatively charged with below -50mV. Generally, it is considered the dispersion is stable when the absolute value of Zeta potential is larger than 30mV because of electrostatic repulsion.<sup>91</sup> This stable GO/rGO dispersion in every condition is attributed to the small size of sheets. Inserted graph in **Figure 27** could support this phenomenon through the comparison between small (~1 $\mu$ m) and large (~10 $\mu$ m) -sized sheets at different pH. Unlike the case of small-sized sheets, Zeta potential of large-sized sheets depends on pH. Cote et al. fabricated this size effect of chemically modified graphene which explains that smaller size of GO sheets are more charged.<sup>3</sup>

We did varied analysis to investigate the phenomenon of GNS formation, but the driving force for spontaneously scrolling process is still unclear. But it is surmised that GNS is formed to minimize the surface energy and this process was affected by pH control. Fan et al. demonstrated that GO could be reduced under alkaline conditions, and they used NaOH which is strong alkali. Given their result, our GO could also be reduced under alkaline conditions even though we used weak alkali, NH<sub>4</sub>OH. Although this reduction procedure with pH control has abnormal analysis results, this mild reduction could affect the chemistry of GO sheets. And consequently, the formation of GNS is caused by this mild reduction.



**Scheme 1** Morphology and formation mechanism of porous graphene nanostructure depending on pH. Most functional groups except for carboxyl groups on GO are reduced after hydrazine reduction, and this residual functional groups are crucial factor for the formation of different morphology depending on pH conditions.

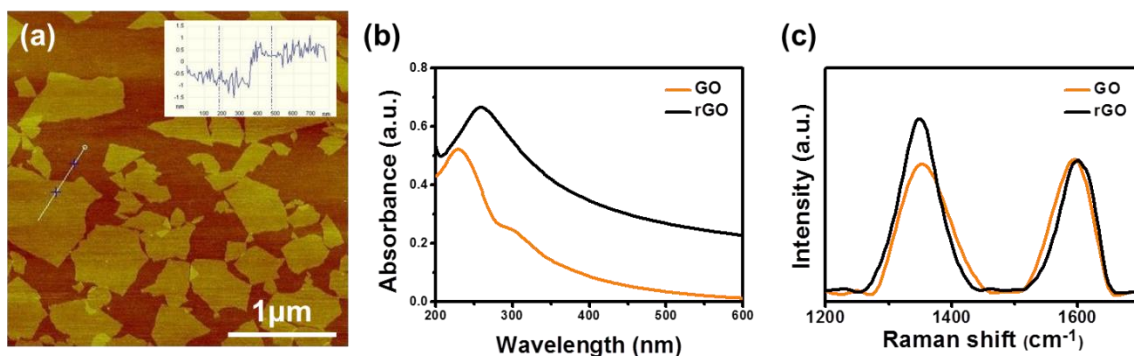


**Figure 8** Analysis of chemically modified graphene. (a) AFM image of GO; the height and the width of GO sheet is below 1nm and 1 $\mu$ m, (b) UV-vis spectra of GO and rGO; red-shift appears after reduction, (c) Raman spectra of GO and rGO with increased  $I_D/I_G$  ratio.

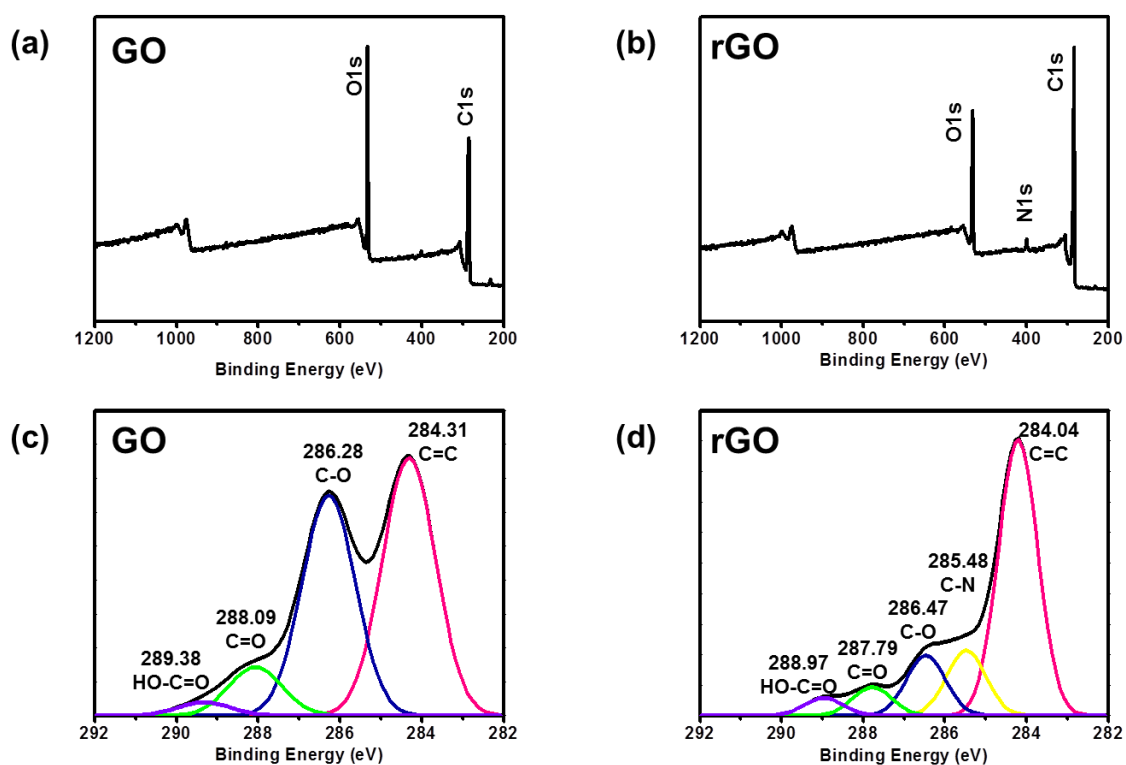


**Figure 9** XPS spectra of GO and rGO. (a-b) wide region: C1s, O1s peaks commonly appear, and N1s peak appear after reduction; (c-d) C1s region: Commonly 4 spectra related to graphitic C=C and functional groups (C-O, C=O, HO-C=O) appear in GO and rGO. Especially in rGO, additional peak with C-N appears.

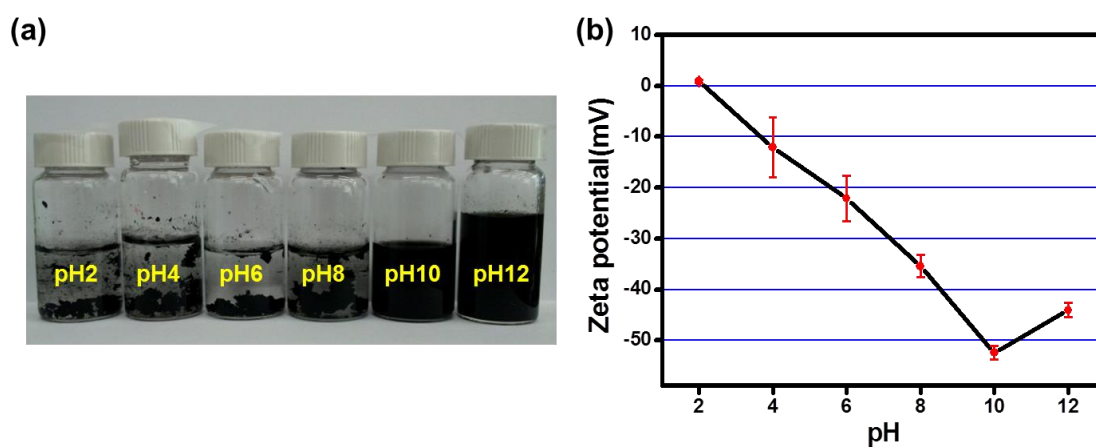


**Figure 10** Change of rGO dispersion as pH conditions from 2 to 12. (a) Formation of agglomerate in rGO dispersion below pH 10, (b) Zeta potential of rGO dispersion as different pH; The most charged state is induced at pH 10.

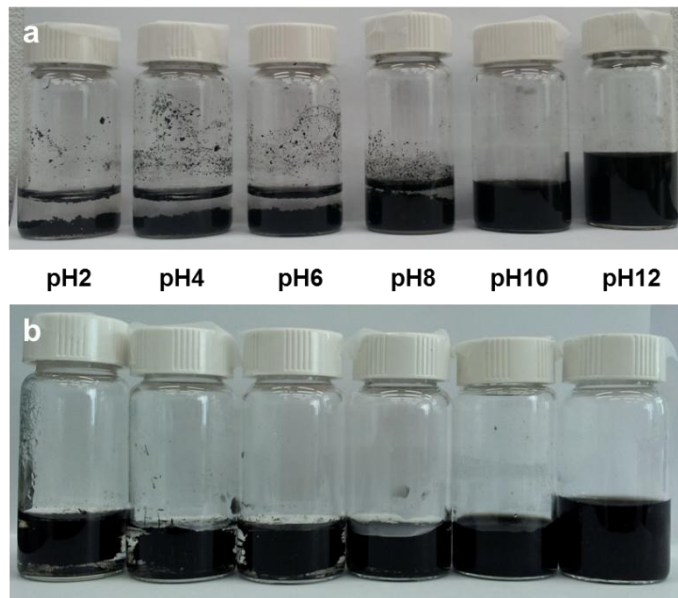


**Figure 11** Photographs of rGO morphology change as varying pH (a) by stirring (SPH and SCH) after a while, and (b) waiting for natural self-assembly (WNH) after near 1 week.



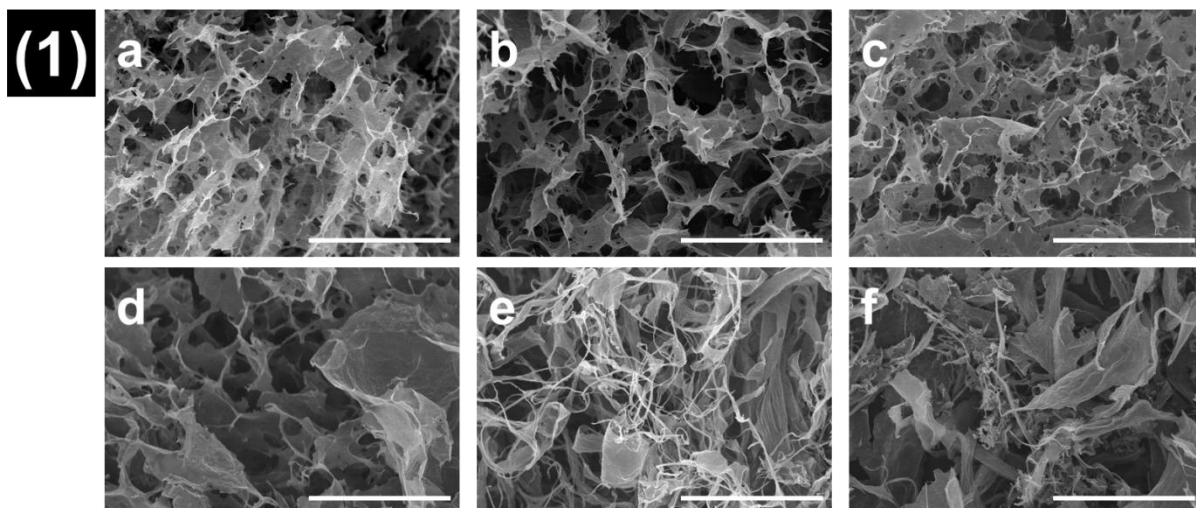


**Figure 12** SEM images of rGO aerogels synthesized by method (1) among the three different approaches at each pH condition; rGO aerogels synthesized by pH control and a wait for natural self-assembly for hydrogel (WNH) (pH2, 4, 6, 8, 10, 12 in alphabetical order; every scale bar: 50  $\mu\text{m}$ ); The morphology of rGO aerogels depend on pH conditions, indicating the dendrite-like structure is shown below pH 10, the wire-like structure appears at pH10, the structure above pH10 is out of tendency.

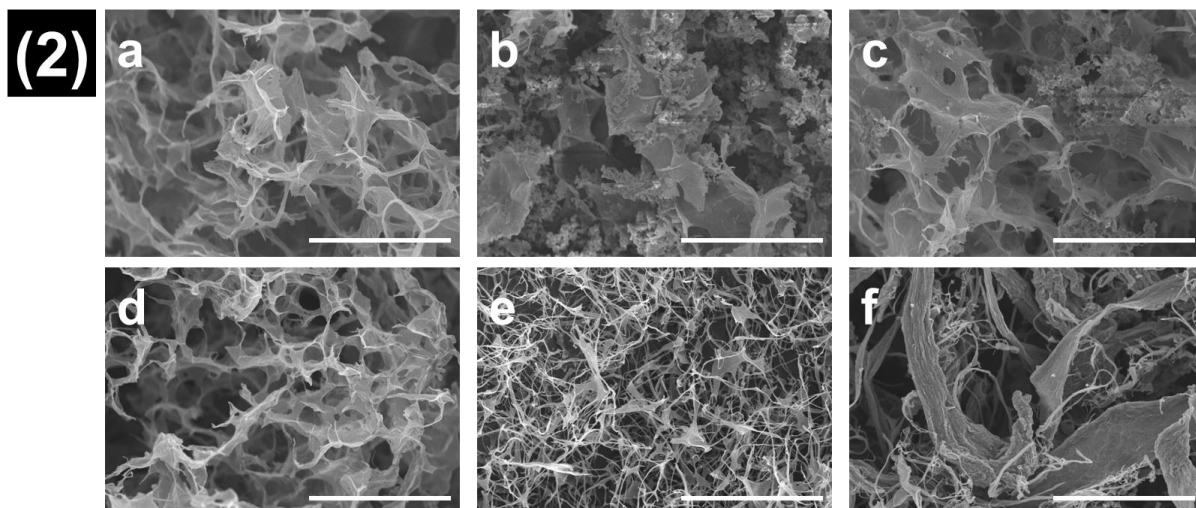


**Figure 13** SEM images of rGO aerogels synthesized by method (2) among the three different approaches at each pH condition; rGO aerogel synthesized by stirring and extracting the supernatant by pipetting (SPH) (pH2, 4, 6, 8, 10, 12 in alphabetical order; every scale bar: 50  $\mu\text{m}$ ); The morphology of rGO aerogels depend on pH conditions, indicating the dendrite-like structure is shown below pH 10, the wire-like structure appears at pH10, the structure above pH10 is out of tendency.

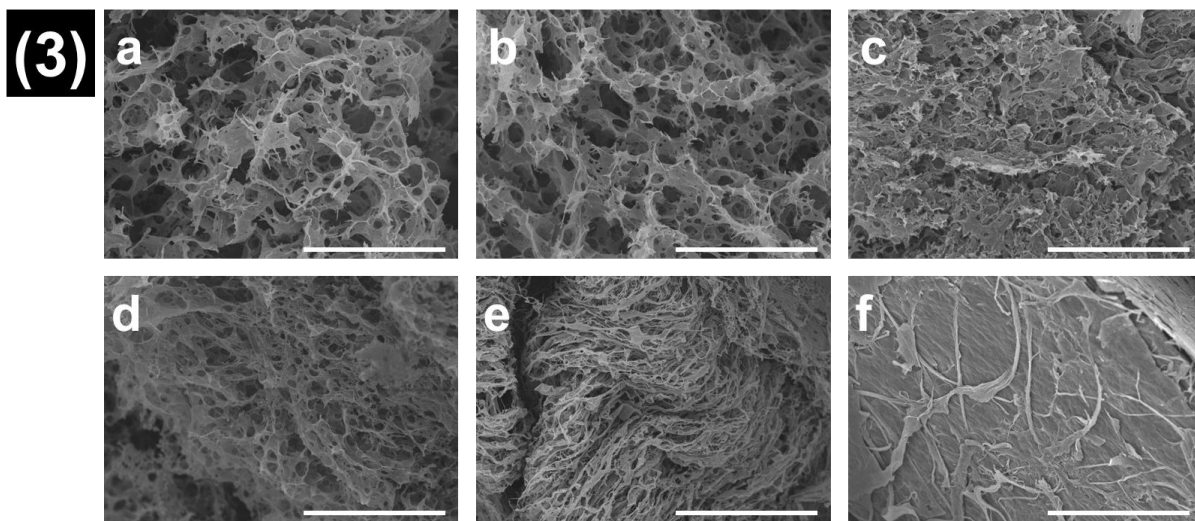


**Figure 14** SEM images of rGO aerogels synthesized by method (3) among the three different approaches at each pH condition; rGO aerogels synthesized by stirring and extracting the supernatant by centrifuge for hydrogel (SCH) (pH2, 4, 6, 8, 10, 12 in alphabetical order; every scale bar: 50  $\mu\text{m}$ ); The morphology of rGO aerogels depend on pH conditions, indicating the dendrite-like structure is shown below pH 10, the wire-like structure appears at pH10, the structure above pH10 is out of tendency.

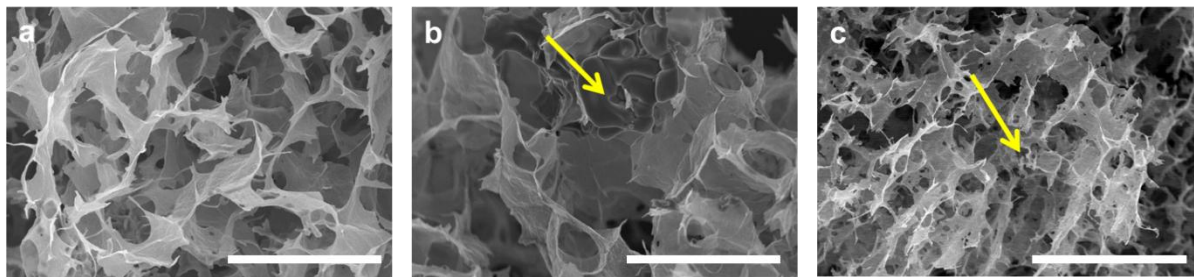


**Figure 15** Effect of salts in each rGO aerogel synthesized by (a) approach with pH control by stirring and separation by centrifuge (SCH), (b) approach with pH control by stirring and separation by pipette (SPH), and (c) approach with pH control and a wait for natural self-assembly (WNH). The salts noticeably appear in SPH and WNH, but hardly appear in SCH. The salts are pointed out with yellow arrows.

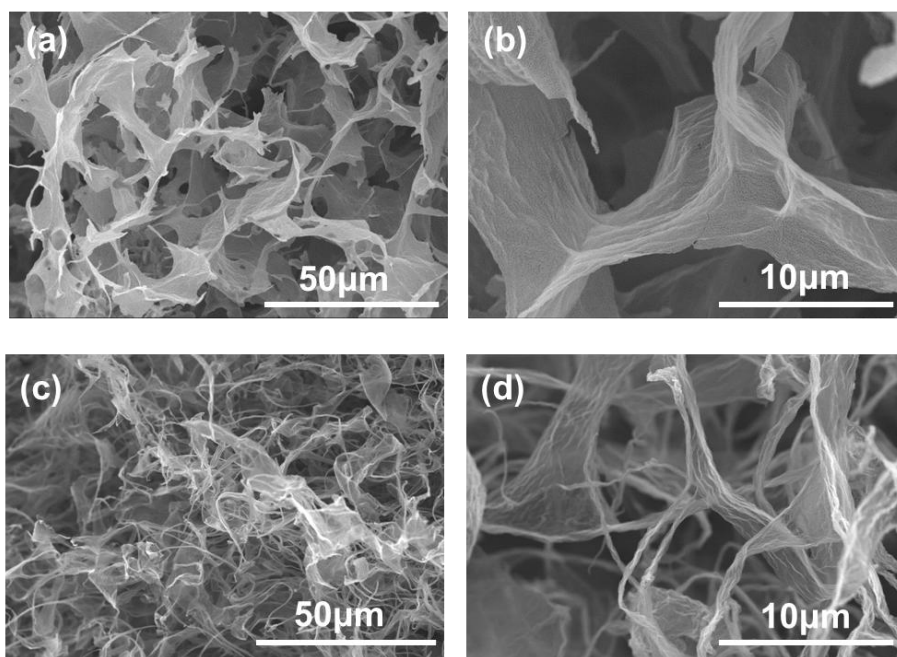


**Figure 16** (a-d) SEM images of rGO aerogel induced by stirring and centrifuge (SCH); (a-b) dendrite-like structure at pH2, (c-d) fiber-like structure at pH10.

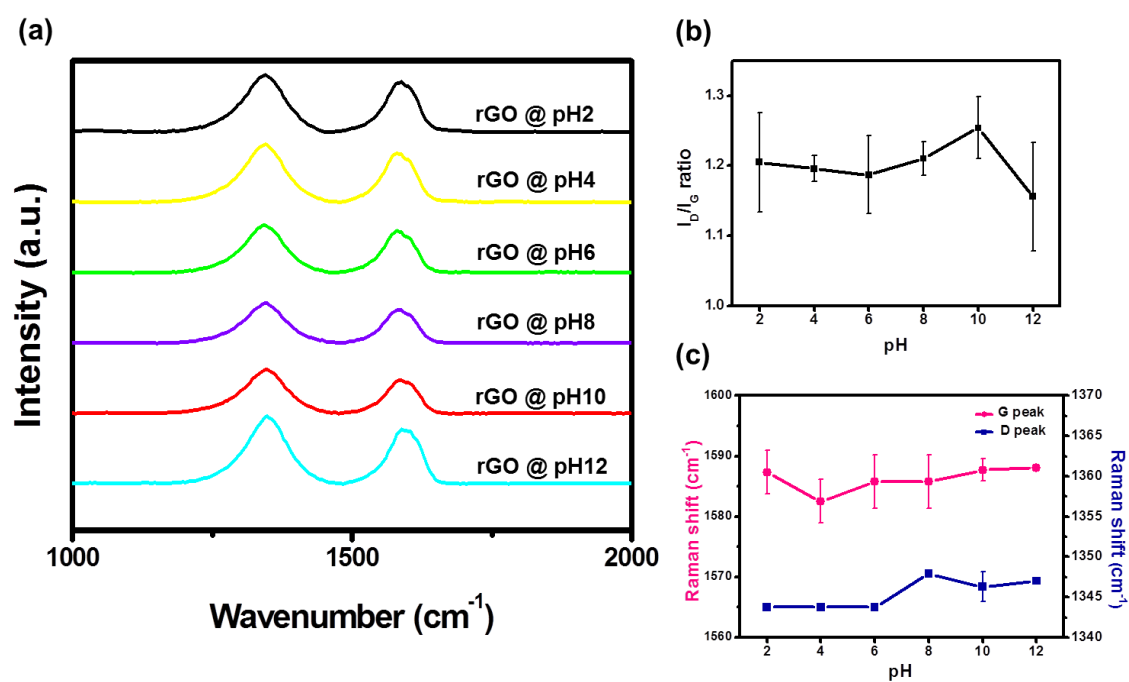


**Figure 17** Raman spectra of rGO aerogels as changing pH; (a) D peak (~1345cm<sup>-1</sup>) and G peak (~1585cm<sup>-1</sup>) are similarly shown in each pH conditions, (b) I<sub>D</sub>/I<sub>G</sub> ratio and (c) position of both peaks as changing pH conditions. Entire data is not distinct from each other.

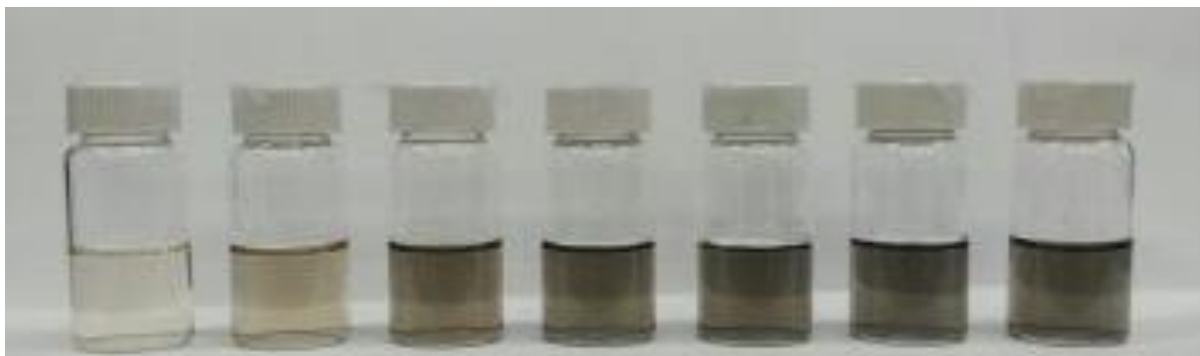


**Figure 18** Color change from yellow to black as controlling pH and reduction time: From left, GO at pH3, pH10, rGO at pH 10 after 0.25h reduction, 0.5h reduction, 1h reduction, 1.5h reduction, 2h reduction. This is indicating the reduction is processed well.

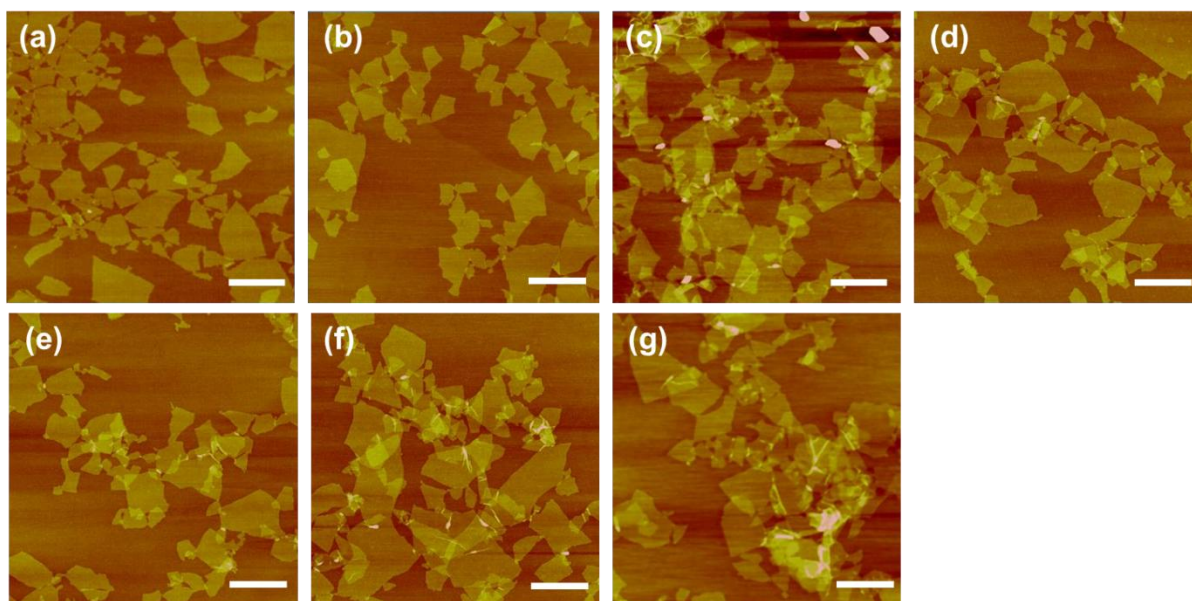


**Figure 19** AFM images with (a) GO at pH3, (b) GO at pH10, and rGO after reduction with (c) 0.25h, (d) 0.5h, (e) 1h, (f) 1.5h, (g) 2h. (Every scale bar: 1  $\mu$ m) While GO sheets are isolated from each other due to functional groups on basal plane such as hydroxyl and epoxy groups, rGO sheets are overlapped because of reduction of functional groups on basal plane.



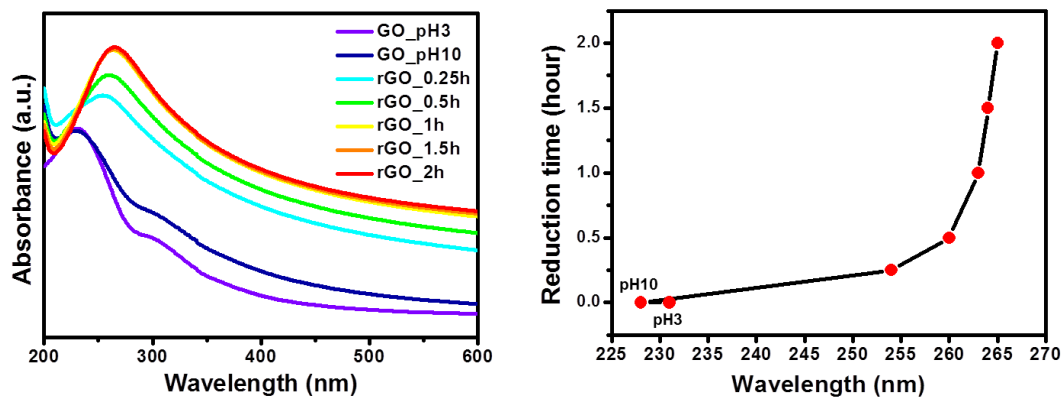


**Figure 20** UV-vis absorption spectra of GO and rGO; (a) UV-vis spectra of each graphene derivative, (b) Change of peak position after control of pH and reduction time. The peak of GO is red-shifted as reduction goes on, but the peak with GO is rather a little blue-shifted after pH control from 3 to 10.

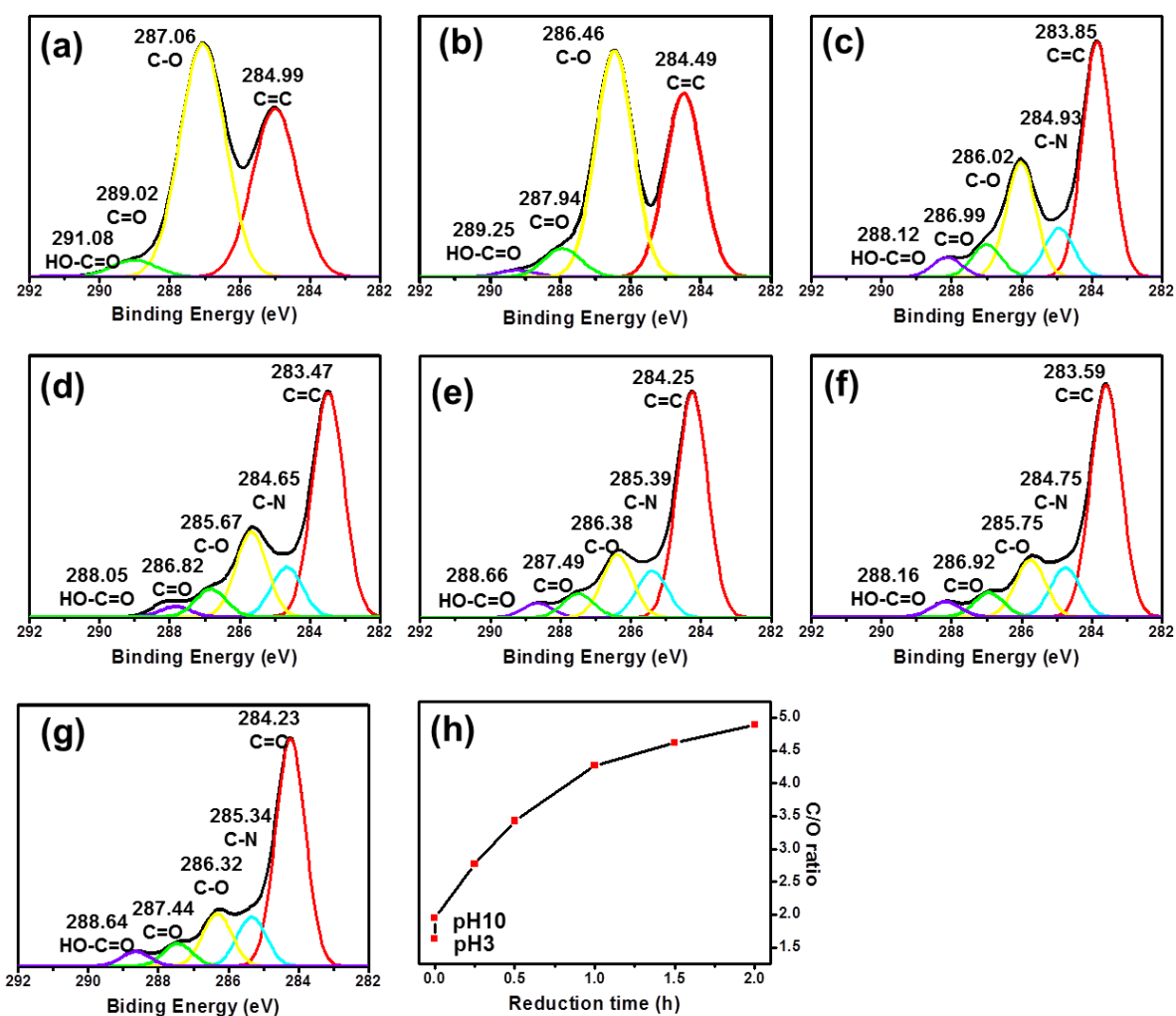


**Figure 21** XPS analysis with GO and rGO; (a-b) Deconvoluted XPS spectra of GO at (a) pH3, (b) pH10; (c-g) Deconvoluted XPS spectra of rGO after (c) 0.25h, (d) 0.5h, (e) 1h, (f) 1.5h, (g) 2h reduction; (h) Change of C/O ratio as control of pH and reduction time; C/O ratio increases as reduction is processed, and after changing pH from 3 to 10.

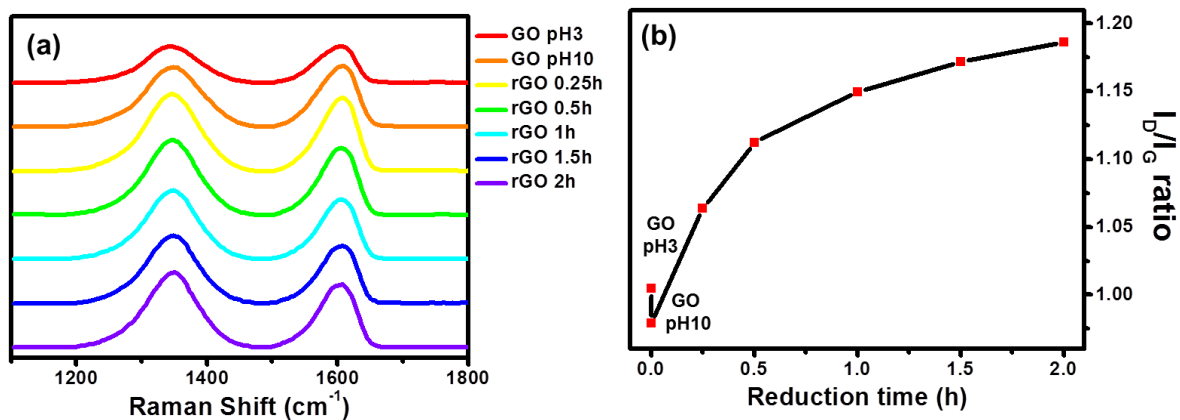
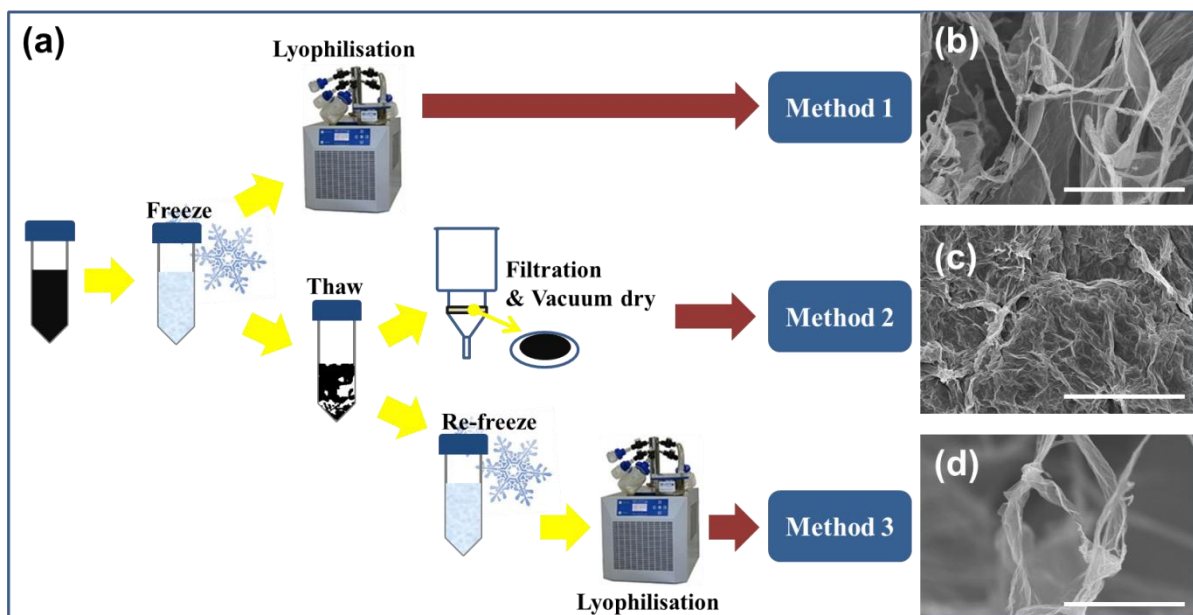


**Figure 22** Raman analysis of GO and rGO. (a) Raman spectra of each graphene derivative. (b)  $I_D/I_G$  ratio after change of pH and reduction time. The positions of D and G peaks at each pH conditions are not differ from each other. While  $I_D/I_G$  ratio is increased as reduction is processed, it is decreased after changing pH condition from 3 to 10.



**Scheme 2** Three approaches for synthesis of GNS; (a) Schematic of each procedure: In method 1, frozen rGO dispersion is under lyophilisation. And rGO film is obtained through filtration of thawed rGO dispersion including agglomeration in method 2. And thawed rGO dispersion is under re-freeze procedure and followed by lyophilisation in method 3; (b-d) SEM images of (b) GNS induced by method 1, (c) a film including GNS induced by method 2, (d) GNS induced by method 3.

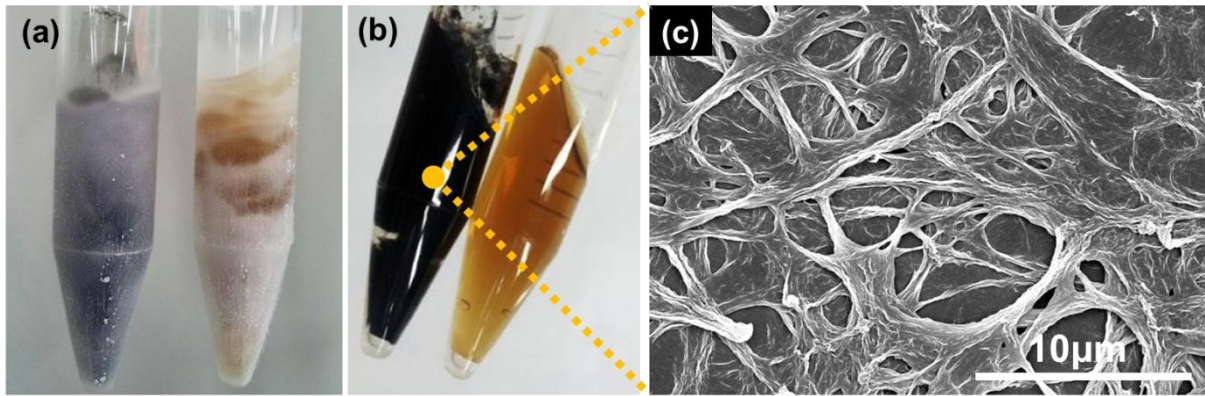


**Figure 23** Freezing-Thawing of GO and rGO. (a) Frozen rGO dispersion(left) and GO dispersion(right), (b) thawed rGO dispersion with agglomeration(left) which has agglomeration, and GO dispersion (right) which is completely re-dispersed, (c) SEM image of thawed rGO agglomeration, indicating scrolled structures are partially shown.

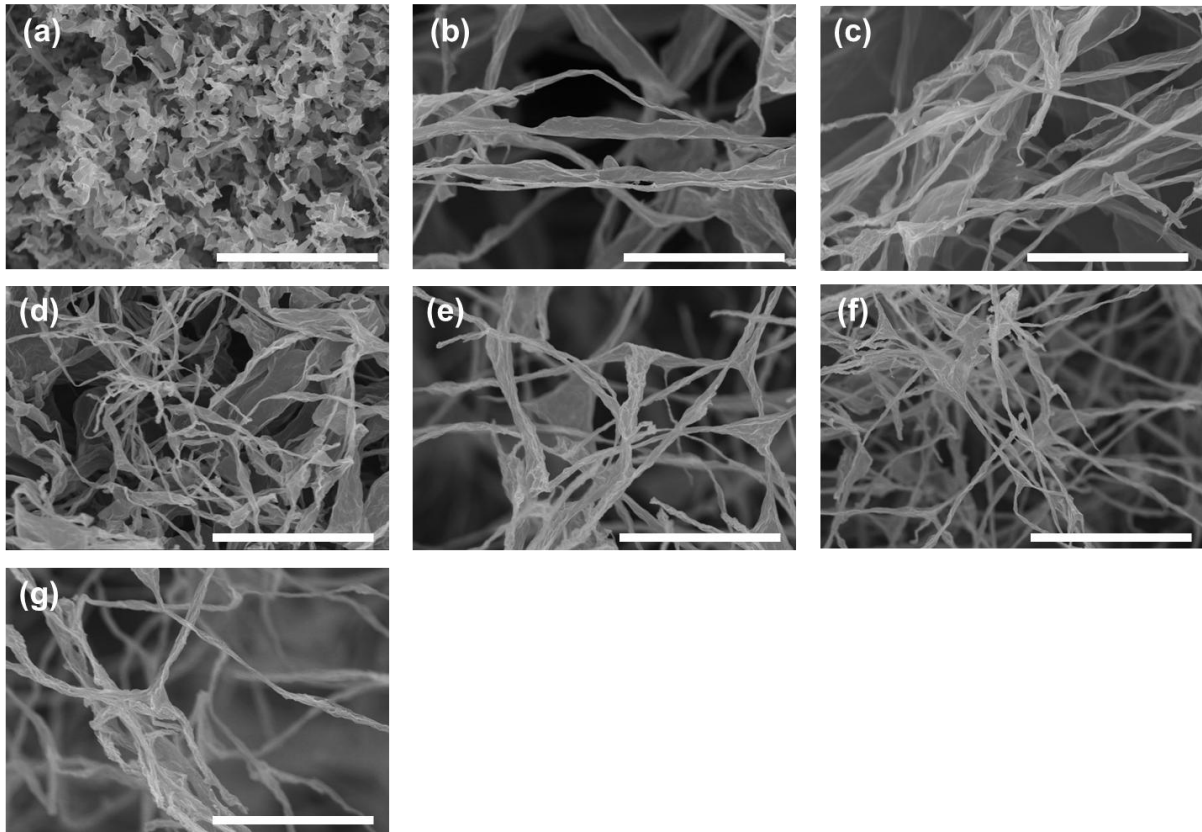


**Figure 24** SEM images of GO at (a) pH3, (b) pH10, and rGO at pH10 after (c) 0.25h, (d) 0.5h, (e) 1h, (f) 1.5h, (g) 2h reduction: All of Scale bars are 10 $\mu$ m. After changing pH condition, scrolled morphology is shown in common.

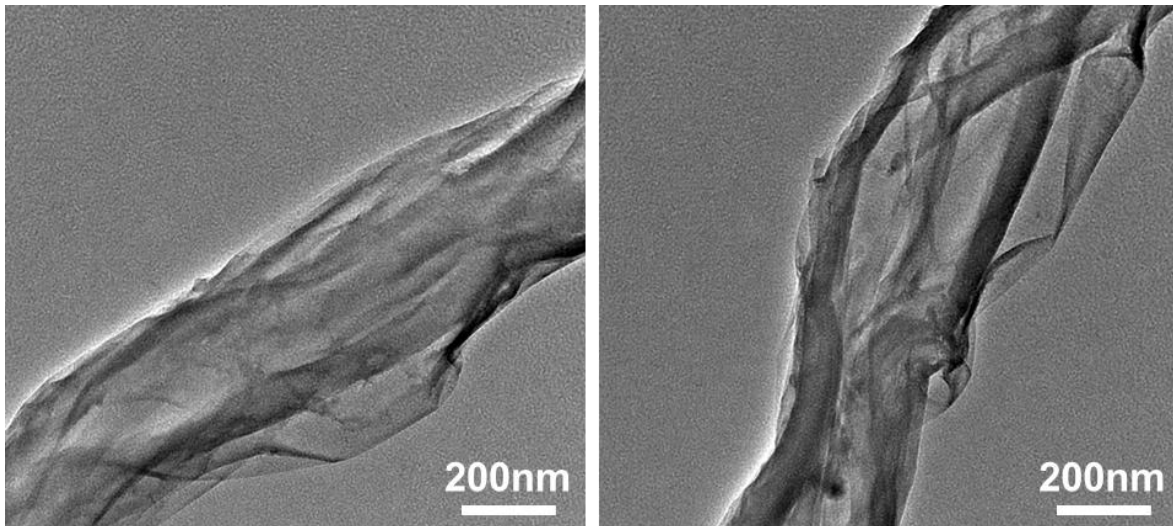
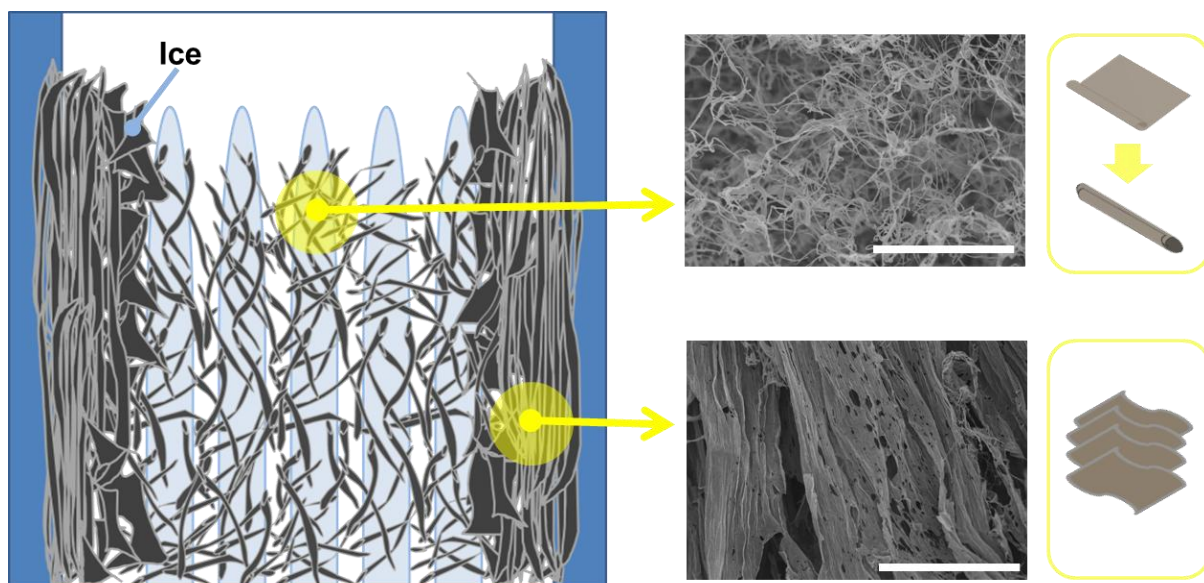


**Figure 25** TEM images of GNS, showing the scrolled state in GNS. This GNS is obtained from rGO aerogel at pH10 after 2h reduction.



**Scheme 3** Morphology and formation mechanism of GNS in polypropylene tube during Lyophilisation (Every scale bar: 50 $\mu$ m); While GNS is formed in the boundary of ice crystals, the stacked thick rGO structure is formed near the wall of polypropylene tube.



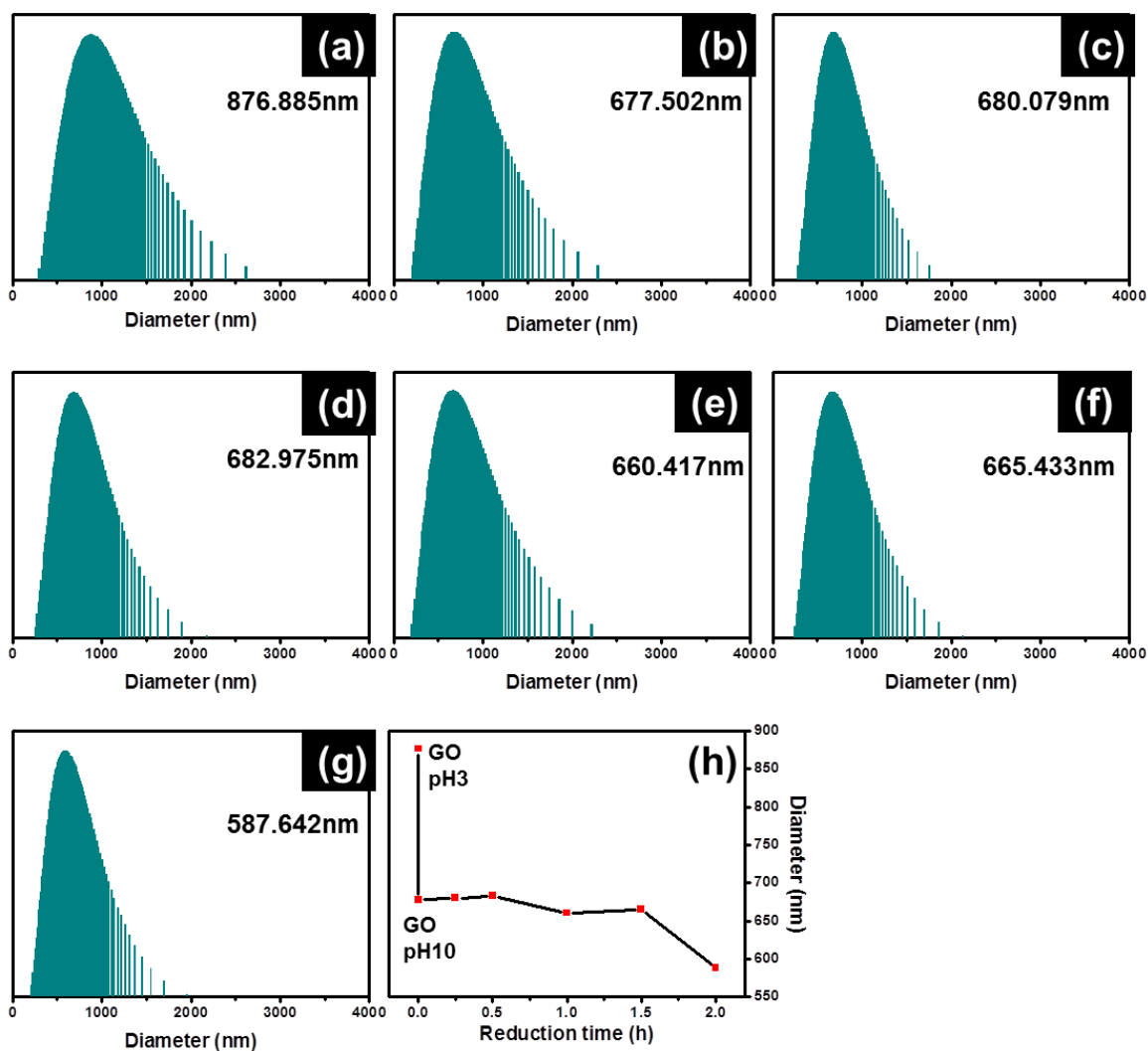


**Figure 26** Dynamic light scattering (DLS) analysis of graphene derivatives: GO at (a) pH3, (b) pH10, and rGO at pH10 after (c) 0.25h, (d) 0.5h, (e) 1h, (f) 1.5h, (g) 2h reduction. (h) Change of diameter as variation in conditions with pH and reduction time. The size of GO or rGO sheets is remarkably decreased after pH change from 3 to 10, while the size is similar to each other in the other conditions.

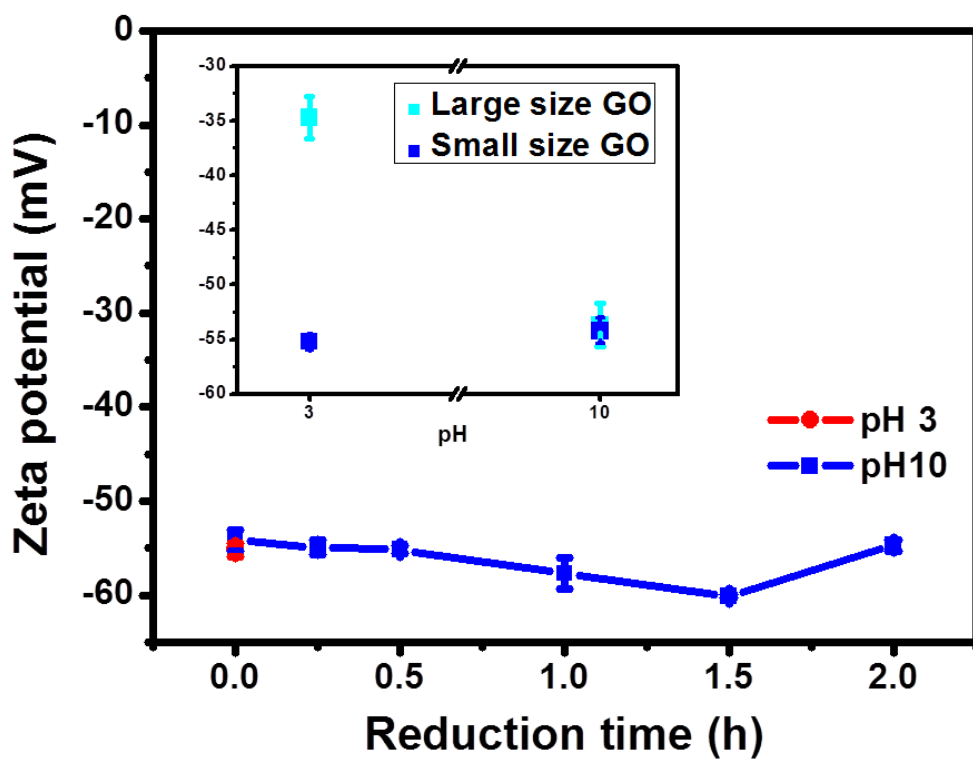


**Figure 27** Zeta potential analysis of graphene derivatives with small sized GO sheets ( $\sim 1\mu\text{m}$ ); inset: comparison of Zeta potential between large sized GO ( $\sim 10\mu\text{m}$ ) and small sized GO ( $\sim 1\mu\text{m}$ ) at different pH. Zeta potential of large sized GO depends on pH conditions, but there is no outstanding change even after pH control and reduction.

## 4. Summary

In summary, porous graphene structures and GNS were induced by the control of pH conditions using chemically modified graphene. Since GO and rGO have functional groups on the surface, they are susceptible to pH conditions. While the functional groups on surface of graphene are deprotonated in base condition, they are protonated in acidic condition. As a result, rGO sheets are crumpled at pH2 because of strong hydrophobicity and  $\pi$ - $\pi$  interaction, whereas rGO sheets are scrolled at pH10 because of modified surface chemistry. Especially, this GNS is affected with pH condition, because even GO sheet is also scrolled at pH10. It is surmised that this scrolling phenomenon is attributed to the mild reduction with alkali,  $\text{NH}_4\text{OH}$ . Consequently, this driving force for formation of GNS is also related to surface chemistry of GO and rGO. Chemically modified graphene is scrolled to be stable with low surface energy, which is associated with varied driving force such as van der Waals force,  $\pi$ - $\pi$  interaction, and hydrophobic/hydrophilic properties.

## 5. Reference

1. Geim, A. K.; Novoselov, K. S., The rise of graphene. *Nature materials* 2007, 6, 183-191.
2. Li, D.; Müller, M. B.; Gilje, S.; Kaner, R. B.; Wallace, G. G., Processable aqueous dispersions of graphene nanosheets. *Nature nanotechnology* 2008, 3, 101-105.
3. Cote, L. J.; Kim, J.; Tung, V. C.; Luo, J. Y.; Kim, F.; Huang, J. X., Graphene oxide as surfactant sheets. *Pure and Applied Chemistry* 2011, 83, 95-110.
4. Kosynkin, D. V.; Higginbotham, A. L.; Sinitskii, A.; Lomeda, J. R.; Dimiev, A.; Price, B. K.; Tour, J. M., Longitudinal unzipping of carbon nanotubes to form graphene nanoribbons. *Nature* 2009, 458, 872-876.
5. Braga, S. F.; Coluci, V. R.; Legoas, S. B.; Giro, R.; Galvão, D. S.; Baughman, R. H., Structure and dynamics of carbon nanoscrolls. *Nano letters* 2004, 4, 881-884.
6. Kim, J.; Kim, F.; Huang, J., Seeing graphene-based sheets. *Materials today* 2010, 13, 28-38.
7. Bonaccorso, F.; Lombardo, A.; Hasan, T.; Sun, Z.; Colombo, L.; Ferrari, A. C., Production and processing of graphene and 2d crystals. *Materials Today* 2012, 15, 564-589.
8. Huang, X.; Qian, K.; Yang, J.; Zhang, J.; Li, L.; Yu, C.; Zhao, D., Functional Nanoporous Graphene Foams with Controlled Pore Sizes. *Advanced Materials* 2012, 24, 4419-4423.
9. Xiao, J.; Mei, D.; Li, X.; Xu, W.; Wang, D.; Graff, G. L.; Bennett, W. D.; Nie, Z.; Saraf, L. V.; Aksay, I. A., Hierarchically porous graphene as a lithium-air battery electrode. *Nano letters* 2011, 11, 5071-5078.
10. Yang, S.-Y.; Chang, K.-H.; Tien, H.-W.; Lee, Y.-F.; Li, S.-M.; Wang, Y.-S.; Wang, J.-Y.; Ma, C.-C. M.; Hu, C.-C., Design and tailoring of a hierarchical graphene-carbon nanotube architecture for supercapacitors. *J. Mater. Chem.* 2010, 21, 2374-2380.
11. Ji, H.; Zhang, L.; Pettes, M. T.; Li, H.; Chen, S.; Shi, L.; Piner, R.; Ruoff, R. S., Ultrathin Graphite Foam: A Three-Dimensional Conductive Network for Battery Electrodes. *Nano letters* 2012, 12, 2446-2451.
12. Zhang, F.; Zhang, X.; Dong, Y.; Wang, L., Facile and effective synthesis of reduced graphene oxide encapsulated sulfur via oil/water system for high performance lithium sulfur cells. *Journal of Materials Chemistry* 2012, 22, 11452-11454.
13. Viculis, L. M.; Mack, J. J.; Kaner, R. B., A chemical route to carbon nanoscrolls. *Science* 2003, 299, 1361-1361.
14. Zheng, J.; Liu, H.; Wu, B.; Guo, Y.; Wu, T.; Yu, G.; Liu, Y.; Zhu, D., Production of High-Quality Carbon Nanoscrolls with Microwave Spark Assistance in Liquid Nitrogen. *Advanced Materials* 2011, 23, 2460-2463.
15. Xie, X.; Ju, L.; Feng, X.; Sun, Y.; Zhou, R.; Liu, K.; Fan, S.; Li, Q.; Jiang, K., Controlled

- fabrication of high-quality carbon nanoscrolls from monolayer graphene. *Nano letters* 2009, 9, 2565-2570.
16. Novoselov, K.; Geim, A.; Morozov, S.; Jiang, D.; Zhang, Y.; Dubonos, S.; Grigorieva, I.; Firsov, A., Electric field effect in atomically thin carbon films. *Science* 2004, 306, 666-669.
  17. Novoselov, K.; Geim, A.; Morozov, S.; Jiang, D.; Grigorieva, M. I. K. I. V.; Dubonos, S.; Firsov, A., Two-dimensional gas of massless Dirac fermions in graphene. *Nature* 2005, 438, 197-200.
  18. Bolotin, K. I.; Sikes, K. J.; Jiang, Z.; Klima, M.; Fudenberg, G.; Hone, J.; Kim, P.; Stormer, H. L., Ultrahigh electron mobility in suspended graphene. *Solid State Communications* 2008, 146, 351-355.
  19. Lee, C.; Wei, X.; Kysar, J. W.; Hone, J., Measurement of the elastic properties and intrinsic strength of monolayer graphene. *Science* 2008, 321, 385-388.
  20. Morozov, S.; Novoselov, K.; Katsnelson, M.; Schedin, F.; Elias, D.; Jaszczak, J.; Geim, A., Giant intrinsic carrier mobilities in graphene and its bilayer. *Physical review letters* 2008, 100, 16602.
  21. Tang, Z.; Shen, S.; Zhuang, J.; Wang, X., Noble-Metal-Promoted Three-Dimensional Macroassembly of Single-Layered Graphene Oxide. *Angewandte Chemie* 2010, 122, 4707-4711.
  22. Li, X.; Cai, W.; An, J.; Kim, S.; Nah, J.; Yang, D.; Piner, R.; Velamakanni, A.; Jung, I.; Tutuc, E., Large-area synthesis of high-quality and uniform graphene films on copper foils. *Science* 2009, 324, 1312-1314.
  23. Fowler, J. D.; Allen, M. J.; Tung, V. C.; Yang, Y.; Kaner, R. B.; Weiller, B. H., Practical chemical sensors from chemically derived graphene. *ACS nano* 2009, 3, 301-306.
  24. Schedin, F.; Geim, A.; Morozov, S.; Hill, E.; Blake, P.; Katsnelson, M.; Novoselov, K., Detection of individual gas molecules adsorbed on graphene. *Nature materials* 2007, 6, 652-655.
  25. Shao, Y.; Wang, J.; Wu, H.; Liu, J.; Aksay, I. A.; Lin, Y., Graphene based electrochemical sensors and biosensors: a review. *Electroanalysis* 2010, 22, 1027-1036.
  26. Worsley, M. A.; Pauzuskie, P. J.; Olson, T. Y.; Biener, J.; Satcher Jr, J. H.; Baumann, T. F., Synthesis of graphene aerogel with high electrical conductivity. *Journal of the American Chemical Society* 2010, 132, 14067-14069.
  27. Vollmer, A.; Feng, X.; Wang, X.; Zhi, L.; Müllen, K.; Koch, N.; Rabe, J., Electronic and structural properties of graphene-based transparent and conductive thin film electrodes. *Applied Physics A: Materials Science & Processing* 2009, 94, 1-4.
  28. Yoo, E. J.; Kim, J.; Hosono, E.; Zhou, H.; Kudo, T.; Honma, I., Large reversible Li storage of graphene nanosheet families for use in rechargeable lithium ion batteries. *Nano letters* 2008,

- 8, 2277-2282.
29. Wang, X.; Zhi, L.; Müllen, K., Transparent, conductive graphene electrodes for dye-sensitized solar cells. *Nano letters* 2008, 8, 323-327.
  30. Vivekchand, S. R. C.; Rout, C. S.; Subrahmanyam, K.; Govindaraj, A.; Rao, C. N. R., Graphene-based electrochemical supercapacitors. *Journal of Chemical Sciences* 2008, 120, 9-13.
  31. Eda, G.; Fanchini, G.; Chhowalla, M., Large-area ultrathin films of reduced graphene oxide as a transparent and flexible electronic material. *Nature nanotechnology* 2008, 3, 270-274.
  32. Hass, J.; De Heer, W.; Conrad, E., The growth and morphology of epitaxial multilayer graphene. *Journal of Physics: Condensed Matter* 2008, 20, 323202.
  33. Reina, A.; Jia, X.; Ho, J.; Nezich, D.; Son, H.; Bulovic, V.; Dresselhaus, M. S.; Kong, J., Large area, few-layer graphene films on arbitrary substrates by chemical vapor deposition. *Nano letters* 2008, 9, 30-35.
  34. Jaber-Ansari, L.; Hersam, M. C., Solution-processed graphene materials and composites. *MRS bulletin* 2012, 37, 1167-1175.
  35. Park, S.; Ruoff, R. S., Chemical methods for the production of graphenes. *Nature nanotechnology* 2009, 4, 217-224.
  36. Jiao, L.; Wang, X.; Diankov, G.; Wang, H.; Dai, H., Facile synthesis of high-quality graphene nanoribbons. *Nature nanotechnology* 2010, 5, 321-325.
  37. Schafhaeutl, C., On the combinations of carbon with silicon and iron, and other metals, forming the different species of cast iron, steel, and malleable iron. *The London and Edinburgh Philosophical Magazine and Journal of Science* 1840, 16, 570-590.
  38. Brodie, B., Sur le poids atomique du graphite. *Ann. Chim. Phys* 1860, 59.
  39. Staudenmaier, L., Verfahren zur darstellung der graphitsäure. *Berichte der deutschen chemischen Gesellschaft* 1898, 31, 1481-1487.
  40. Hummers, W. S.; Offeman, R. E., Preparation of Graphitic Oxide. *Journal of the American Chemical Society* 1958, 80, 1339-1339.
  41. Kovtyukhova, N. I.; Ollivier, P. J.; Martin, B. R.; Mallouk, T. E.; Chizhik, S. A.; Buzaneva, E. V.; Gorchinskiy, A. D., Layer-by-layer assembly of ultrathin composite films from micron-sized graphite oxide sheets and polycations. *Chemistry of materials* 1999, 11, 771-778.
  42. Hirata, M.; Gotou, T.; Horiuchi, S.; Fujiwara, M.; Ohba, M., Thin-film particles of graphite oxide 1:: High-yield synthesis and flexibility of the particles. *Carbon* 2004, 42, 2929-2937.
  43. Xu, Y.; Bai, H.; Lu, G.; Li, C.; Shi, G., Flexible graphene films via the filtration of water-soluble noncovalent functionalized graphene sheets. *Journal of the American Chemical Society* 2008, 130, 5856-5857.
  44. Jo, K.; Lee, T.; Choi, H. J.; Park, J. H.; Lee, D. J.; Lee, D. W.; Kim, B.-S., Stable Aqueous

- Dispersion of Reduced Graphene Nanosheets via Non-Covalent Functionalization with Conducting Polymers and Application in Transparent Electrodes. *Langmuir* 2011, 27, 2014-2018.
45. Compton, O. C.; Nguyen, S. T., Graphene Oxide, Highly Reduced Graphene Oxide, and Graphene: Versatile Building Blocks for Carbon-Based Materials. *Small* 2010, 6, 711-723.
  46. Park, S.; Ruoff, R. S., Chemical methods for the production of graphenes *Nature nanotechnology* 2010, 5, 309-309.
  47. Gómez-Navarro, C.; Weitz, R. T.; Bittner, A. M.; Scolari, M.; Mews, A.; Burghard, M.; Kern, K., Electronic transport properties of individual chemically reduced graphene oxide sheets. *Nano letters* 2007, 7, 3499-3503.
  48. Becerril, H. A.; Mao, J.; Liu, Z.; Stoltenberg, R. M.; Bao, Z.; Chen, Y., Evaluation of solution-processed reduced graphene oxide films as transparent conductors. *ACS nano* 2008, 2, 463-470.
  49. Gilje, S.; Han, S.; Wang, M.; Wang, K. L.; Kaner, R. B., A chemical route to graphene for device applications. *Nano Letters* 2007, 7, 3394-3398.
  50. Moon, I. K.; Kim, J. I.; Lee, H.; Hur, K.; Kim, W. C.; Lee, H., 2D Graphene Oxide Nanosheets as an Adhesive Over-Coating Layer for Flexible Transparent Conductive Electrodes. *Scientific reports* 2013, 3.
  51. Cote, L. J.; Kim, F.; Huang, J., Langmuir-Blodgett assembly of graphite oxide single layers. *J. Am. Chem. Soc* 2009, 131, 1043-1049.
  52. Li, X.; Zhang, G.; Bai, X.; Sun, X.; Wang, X.; Wang, E.; Dai, H., Highly conducting graphene sheets and Langmuir-Blodgett films. *Nature nanotechnology* 2008, 3, 538-542.
  53. Kim, J.; Cote, L. J.; Kim, F.; Yuan, W.; Shull, K. R.; Huang, J., Graphene oxide sheets at interfaces. *Journal of the American Chemical Society* 2010, 132, 8180-8186.
  54. Robinson, J. T.; Zalalutdinov, M.; Baldwin, J. W.; Snow, E. S.; Wei, Z.; Sheehan, P.; Houston, B. H., Wafer-scale reduced graphene oxide films for nanomechanical devices. *Nano letters* 2008, 8, 3441-3445.
  55. Eda, G.; Chhowalla, M., Chemically Derived Graphene Oxide: Towards Large-Area Thin-Film Electronics and Optoelectronics. *Advanced materials* 2010, 22, 2392-2415.
  56. Tao, Y.; Endo, M.; Inagaki, M.; Kaneko, K., Recent progress in the synthesis and applications of nanoporous carbon films. *J. Mater. Chem.* 2010, 21, 313-323.
  57. Li, C.; Shi, G., Three-dimensional graphene architectures. *Nanoscale* 2012, 4, 5549-5563.
  58. Choi, B. G.; Yang, M. H.; Hong, W. H.; Choi, J. W.; Huh, Y. S., 3D Macroporous Graphene Frameworks for Supercapacitors with High Energy and Power Densities. *ACS nano* 2012, 6, 4020-4028.
  59. Chen, Z.; Ren, W.; Gao, L.; Liu, B.; Pei, S.; Cheng, H. M., Three-dimensional flexible and

- conductive interconnected graphene networks grown by chemical vapour deposition. *Nature materials* 2011, 10, 424-428.
60. Kim, K. H.; Oh, Y.; Islam, M., Graphene coating makes carbon nanotube aerogels superelastic and resistant to fatigue. *Nature nanotechnology* 2012.
  61. Xu, Y.; Sheng, K.; Li, C.; Shi, G., Self-assembled graphene hydrogel via a one-step hydrothermal process. *ACS nano* 2010, 4, 4324-4330.
  62. Wu, Z.-S.; Yang, S.; Sun, Y.; Parvez, K.; Feng, X.; Müllen, K., 3D Nitrogen-Doped Graphene Aerogel-Supported Fe<sub>3</sub>O<sub>4</sub> Nanoparticles as Efficient Electrocatalysts for the Oxygen Reduction Reaction. *Journal of the American Chemical Society* 2012, 134, 9082-9085.
  63. Cong, H.-P.; Ren, X.-C.; Wang, P.; Yu, S.-H., Macroscopic multifunctional graphene-based hydrogels and aerogels by a metal ion induced self-assembly process. *ACS nano* 2012, 6, 2693-2703.
  64. Chen, P.; Yang, J.-J.; Li, S.-S.; Wang, Z.; Xiao, T.-Y.; Qian, Y.-H.; Yu, S.-H., Hydrothermal synthesis of macroscopic nitrogen-doped graphene hydrogels for ultrafast supercapacitor. *Nano Energy* 2012.
  65. Paek, S.-M.; Yoo, E.; Honma, I., Enhanced cyclic performance and lithium storage capacity of SnO<sub>2</sub>/graphene nanoporous electrodes with three-dimensionally delaminated flexible structure. *Nano Letters* 2008, 9, 72-75.
  66. Yavari, F.; Chen, Z.; Thomas, A. V.; Ren, W.; Cheng, H.-M.; Koratkar, N., High sensitivity gas detection using a macroscopic three-dimensional graphene foam network. *Scientific reports* 2011, 1.
  67. Kong, J.; Franklin, N. R.; Zhou, C.; Chapline, M. G.; Peng, S.; Cho, K.; Dai, H., Nanotube molecular wires as chemical sensors. *Science* 2000, 287, 622-625.
  68. Miasik, J. J.; Hooper, A.; Tofield, B. C., Conducting polymer gas sensors. *J. Chem. Soc., Faraday Trans. 1* 1986, 82, 1117-1126.
  69. Chen, Y.; Lu, J.; Gao, Z., Structural and electronic study of nanoscrolls rolled up by a single graphene sheet. *The Journal of Physical Chemistry C* 2007, 111, 1625-1630.
  70. Pan, H.; Feng, Y.; Lin, J., Ab initio study of electronic and optical properties of multiwall carbon nanotube structures made up of a single rolled-up graphite sheet. *Phys Rev B* 2005, 72, 085415.
  71. Bacon, R., Growth, Structure, and Properties of Graphite Whiskers. *J Appl Phys* 1960, 31, 283-290.
  72. Li, J.; Peng, Q.; Bai, G.; Jiang, W., Carbon scrolls produced by high energy ball milling of graphite. *Carbon* 2005, 43, 2817-2833.
  73. Zeng, F.; Kuang, Y.; Wang, Y.; Huang, Z.; Fu, C.; Zhou, H., Facile Preparation of High-



- Quality Graphene Scrolls from Graphite Oxide by a Microexplosion Method. *Advanced Materials* 2011, 23, 4929-4932.
74. Zeng, F.; Kuang, Y.; Liu, G.; Liu, R.; Huang, Z.; Fu, C.; Zhou, H., Supercapacitors based on high-quality graphene scrolls. *Nanoscale* 2012, 4, 3997-4001.
  75. Shioyama, H.; Akita, T., A new route to carbon nanotubes. *Carbon* 2003, 41, 179-180.
  76. Zhou, W. W.; Liu, J. P.; Chen, T.; Tan, K. S.; Jia, X. T.; Luo, Z. Q.; Cong, C. X.; Yang, H. P.; Li, C. M.; Yu, T., Fabrication of Co<sub>3</sub>O<sub>4</sub>-reduced graphene oxide scrolls for high-performance supercapacitor electrodes. *Physical Chemistry Chemical Physics* 2011, 13, 14462-14465.
  77. SengáTan, K.; MingáLi, C., Fabrication of Co<sub>3</sub>O<sub>4</sub>-reduced graphene oxide scrolls for high-performance supercapacitor electrodes. *Physical Chemistry Chemical Physics* 2011, 13, 14462-14465.
  78. Coluci, V.; Braga, S.; Baughman, R.; Galvao, D., Prediction of the hydrogen storage capacity of carbon nanoscrolls. *Phys Rev B* 2007, 75, 125404.
  79. Mpourmpakis, G.; Tylíanakis, E.; Froudakis, G. E., Carbon nanoscrolls: a promising material for hydrogen storage. *Nano letters* 2007, 7, 1893-1897.
  80. Xu, Z.; Buehler, M. J., Geometry controls conformation of graphene sheets: membranes, ribbons, and scrolls. *ACS nano* 2010, 4, 3869-3876.
  81. Zhu, S.; Li, T., Hydrogenation enabled scrolling of graphene. *Journal of Physics D: Applied Physics* 2013, 46, 075301.
  82. Xia, D.; Xue, Q.; Xie, J.; Chen, H.; Lv, C.; Besenbacher, F.; Dong, M., Fabrication of carbon nanoscrolls from monolayer graphene. *small* 2010, 6.
  83. Wang, X.; Yang, D.-P.; Huang, G.; Huang, P.; Shen, G.; Guo, S.; Mei, Y.; Cui, D., Rolling up graphene oxide sheets into micro/nanoscrolls by nanoparticle aggregation. *J. Mater. Chem.* 2012, 22, 17441-17444.
  84. Tung, V. C.; Allen, M. J.; Yang, Y.; Kaner, R. B., High-throughput solution processing of large-scale graphene. *Nature nanotechnology* 2008, 4, 25-29.
  85. Stankovich, S.; Dikin, D. A.; Piner, R. D.; Kohlhaas, K. A.; Kleinhammes, A.; Jia, Y.; Wu, Y.; Nguyen, S. T.; Ruoff, R. S., Synthesis of graphene-based nanosheets via chemical reduction of exfoliated graphite oxide. *Carbon* 2007, 45, 1558-1565.
  86. Gao, W.; Alemany, L. B.; Ci, L.; Ajayan, P. M., New insights into the structure and reduction of graphite oxide. *Nat Chem* 2009, 1, 403-408.
  87. Lee, V.; Whittaker, L.; Jaye, C.; Baroudi, K. M.; Fischer, D. A.; Banerjee, S., Large-area chemically modified graphene films: electrophoretic deposition and characterization by soft X-ray absorption spectroscopy. *Chemistry of Materials* 2009, 21, 3905-3916.
  88. Wang, R.; Wang, Y.; Xu, C.; Sun, J.; Gao, L., Facile one-step hydrazine-assisted

- solvothermal synthesis of nitrogen-doped reduced graphene oxide: reduction effect and mechanisms. *RSC Advances* 2013, 3, 1194-1200.
89. Park, S.; Hu, Y.; Hwang, J. O.; Lee, E.-S.; Casabianca, L. B.; Cai, W.; Potts, J. R.; Ha, H.-W.; Chen, S.; Oh, J., Chemical structures of hydrazine-treated graphene oxide and generation of aromatic nitrogen doping. *Nature Communications* 2012, 3, 638.
  90. Pei, S.; Cheng, H.-M., The reduction of graphene oxide. *Carbon* 2012, 50, 3210-3228.
  91. Konkena, B.; Vasudevan, S., Understanding Aqueous Dispersibility of Graphene Oxide and Reduced Graphene Oxide through p K a Measurements. *The Journal of Physical Chemistry Letters* 2012, 3, 867-872.
  92. Cote, L. J.; Kim, J.; Tung, V. C.; Luo, J.; Kim, F.; Huang, J., Graphene oxide as surfactant sheets. *Pure and Applied Chemistry* 2010, 83, 95-110.
  93. Qiu, L.; Liu, J. Z.; Chang, S. L.; Wu, Y.; Li, D., Biomimetic superelastic graphene-based cellular monoliths. *Nature communications* 2012, 3, 1241.

## Acknowledgement

먼저, 한결같이 저를 믿고 지원해주신 부모님께 이 논문을 받칩니다. 3남매 중 장녀인 제게 남다른 관심과 기대를 가지셨던 부모님께 항상 자랑스러운 딸이 되고자 노력하며 살았습니다. 하지만 대학 졸업 후, 기대에 부흥하는 좋은 소식을 안겨드리지 못하고, 대학원에 진학하여 또 다시 학업에 매진하게 되어 늘 죄송한 마음을 갖고 있습니다. 항상 감사하는 마음으로 앞으로 더욱 좋은 모습 보여드리겠습니다.

처음 울산과학기술대학교를 선택하면서, 가족과 떨어져 타지인 울산에서의 기숙사 생활이 불가피하다는 점과 역사가 깊지 않은 신생 학교라는 점에 많은 고민을 했습니다. 하지만, 2년 동안의 석사과정을 마무리하며 되돌아보니, 이 곳에서의 연구실 생활이 제게 실보다는 득이 되었던 것 같습니다. 이는 지도 교수님인 고헌협 교수님의 가르침으로부터의 결과라 생각합니다. 지난 2년간, 교수님께서 스스로 동기부여 되어 연구하는 법을 가르쳐주셨습니다. 처음에는 이러한 지도 방식에 적응하는데 어려움이 많았으나, 덕분에 능동적인 연구 자세를 기를 수 있었다고 생각합니다. 또한, 교수님의 연구에 대한 열정과 인간미 넘치는 성품에서도 많은 것을 배웠습니다. 이런 교수님의 영향으로 저희 연구실은 구성원들 간의 사이가 돈독하고 늘 밝은 분위기를 자랑합니다. 처음 연구실을 방문하여 이것저것 묻던 제게 친절한 설명과 조언을 아끼지 않았던 지원 언니, U-SURF 시절부터 서로를 의지하며 2년간의 석사과정을 함께한 세희, 든든한 연구실의 버팀목으로서 늘 연구에 대한 성실함과 열정을 보여주시는 두승 오빠, 연구실의 화목한 분위기를 잘 조율하고 있는 종화, 늘 오피스 제 옆자리를 지키며 기쁜 일, 힘든 일을 함께 해준 부사수 승영이에게 고맙다는 말을 전하고 싶습니다. 또한, 학부생이었지만 연구실 선배였던 성실한 민정이, 성동이, 해피 바이러스를 전파하는 분위기 메이커 호찬이, 각자의 연구 테마에 대한 열정이 대학원생 못지않은 학부생 아영이, 영

오, 영수, 연구실 구성원이 된지 얼마 되지 않았지만 오랫동안 함께 해 온듯한 소연이와 지수. 모두의 덕분에 많은 것을 느끼고 배우며 무사히 2년간의 석사과정을 마칠 수 있었다고 생각합니다. 학업에 관한 배움 외에도 구성원들의 소중함을 느낄 수 있었던 값진 시간이었습니다. 그 동안 감사했습니다. 각자의 위치에서 맡은 바 최선을 다해, 서로의 좋은 소식을 전할 수 있는 날을 기대하겠습니다. Ko 랩 파이팅!!

